Aiding the Search for New Physics Through the Spectroscopy of Diatomic Molecules

A thesis submitted in partial fulfillment of the requirements of a degree of
Bachelor of Arts in
Physics
at
Pomona College

Andreas Biekert
with advisor
Richard J. Mawhorter, Ph.D.
Professor of Physics
Pomona College

July 12, 2016

Abstract

Diatomic molecules serve as an exciting platform for conducting experiments that push the boundaries of experimental physics. Current fundamental physics problems that can be addressed by diatomic molecules include a measurement of the electron electric dipole moment, a repeat measurement of the nuclear anapole moment, and observations of the variation in fundamental constants of physics. The molecule PbF is sensitive to all of these effects, thanks to a pair of low-lying energy states of opposite parity in the ^{207}PbF isotopologue. High precision spectroscopic measurements of PbF help determine molecular parameters important to these experiments and can validate theoretical calculations surrounding fundamental physics effects. A global Dunham fit has been implemented on a data set comprised of 83 high resolution Fourier-transform microwave transitions (including 16 new in this work) and 608 low resolution Fourier-transform infrared transitions across the four stable isotopes of Pb. The reduced mean square of this fit has a value of 4.54, with some remaining systematic errors in the isotopic mass scaling of the model. Preliminary values for the mass-independent Born-Oppenheimer breakdown parameters, $\Delta_{01}^{Pb} = -21.2(2)$ and $\Delta_{00}^{p,Pb} = 108.2(11)$, have been obtained. Preliminary predictions of the near degeneracy of ^{207}PbF $v = 1$ states analogous to those recently discovered in the ground state indicate a spacing of 233.54 MHz, a roughly 12% smaller spacing than observed in the ground state. Similar predictive work on ^{205}PbF utlizing an initial electric field gradient calculation did not find analogous low-lying energy levels of opposite parity.

Acknowledgments

This thesis represents learning experiences I have collected from various educators, collaborators, and colleagues. I would like to thank my research and thesis advisor Professor Richard Mawhorter for introducing me to many of these people and helping me work through countless problems both related and less related to this work. I am also thankful for the spectroscopic wisdom passed on by Dr. Brian Drouin, Dr. Trevor Sears, and Dr. Jens-Uwe Grabow, who have at various times helped me solve specific problems in addition to giving me a broader overview of the science at hand. In addition to his own spectroscopic expertise, Dr. Ewald H. Fink graciously offered up a tour of his lab and his unpublished lead fluoride data for us to work with. Finally, Dr. Lukáš Pašteka kindly provided us with preliminary *ab initio* calculations for our predictive work to enable the final part of the project.

This work also represents first hand collaborative efforts with my fellow students and friends Zach Glassman, Carson Witte, David Sharfi, and Alex Hof, who made research problems seem tractable with both expertise and good humor. Ultimately, my time at Pomona was shaped by the physics department and wider campus around it, and I am grateful to have been a part of these communities during my college years.

Thank you mom and dad for making it all possible.

Contents

1 Introduction **6**

1.1 The Search for the Electric Dipole Moment of the Electron 6

1.2 Interest in PbF 8

2 Electric Dipole Moment Theory **12**

2.1 The Electron Electric Dipole Moment 12

2.1.1 Theoretical Predictions 12

2.1.2 Measuring the Electron EDM 14

2.1.3 Ongoing Experiments 17

2.2 Electric Dipole Moments of Other Fundamental Particles 18

2.2.1 Neutron Electric Dipole Moments 19

2.2.2 Leveraging the Magnetic Quadrupole Moment 20

3 Spectroscopic Structure of PbF **22**

3.1 YbF 22

3.1.1 The Nuclear Electric Quadrupole Moment and the eQq 23

3.2 PbF 24

3.2.1 Structure of PbF 25

3.2.2 Dunham Formulation 28

3.2.3 Potential Applications of PbF 31

4 Spectroscopic Measurements of PbF **33**

4.1 Experimental Details 33

4.1.1 Fourier Transform Microwave Setup 34

4.1.2 Analysis of Raw Microwave Data 36

4.2 Fitting Routine 37

4.3 Results 38

4.3.1 Born-Oppenheimer Breakdown Findings 39

5 Predictive Work **42**

5.1 Predicting Routine 42

5.2 The ^{207}PbF $v = 1$ State 42

5.2.1 Results 43

5.3 The Structure of ^{205}PbF 46

5.3.1 Scaling ^{205}PbF Parameters 46

5.3.2 The Nuclear Quadrupole Moment of ^{205}PbF 46

5.3.3 Results 47

6 Conclusion **49**

A Data **50**

A.1 Fourier-Transform Microwave Data 50

A.2 Fourier-Transform Infrared Data 52

1 Introduction

The Standard Model of physics provides a remarkably accurate account of particle physics. However, it has several shortcomings, illuminated by known phenomena which it cannot explain. One of the most glaring of these shortcomings is the abundance of matter over antimatter in the universe; in the Standard Model, matter and antimatter should be equally abundant and have mostly annihilated long ago. Instead, our universe exists on a foundation of matter and almost no antimatter, demanding we revise our understanding of particle physics to account for this imbalance.

While we don't have a resolution to these problems, our current understanding of particle physics provides some clues. The Standard Model describes particle interactions as possessing three possible fundamental symmetries, in the form of charge conjugation (C), parity conservation (P), and time reversal (T). Each of these symmetries corresponds to a transformation which is classified as even if the transformed process remains unchanged under the the transformation and odd otherwise. One of the central assumptions made by the Standard Model, called the CPT theorem, is that a combination of transformations in all of these symmetries must produce a symmetric result. The Standard Model in its current form allows for symmetry breaking processes, some of which have been experimentally verified, but still does not account for the extent of the observed matter-antimatter imbalance in the universe. The fact that we exist in a universe made of matter suggests that extensions to the Standard Model are required to describe further cases of symmetry-breaking, which has produced a wide variety of theories with various predictions for parity violating (PV) effects.

1.1 The Search for the Electric Dipole Moment of the Electron

One effect that could provide clues for viable extensions to the Standard Model is an electric dipole moment (EDM) of the electron. The Standard Model prediction for the electron EDM is $d_e \sim 10^{-40}$ e cm. It is small because several terms cancel in the Standard Model calculations [1], however, extensions to the Standard Model predict anywhere from this value to almost fifteen orders of magnitude greater, since the same terms in the calculation no longer cancel. This wide range of predictions allows experimental determination of an upper limit of the eEDM value to constrain viable extensions of the Standard Model, as depicted in Figure 1. The current upper limit was placed at $d_e < 8.7 \times 10^{-29}$ e·cm with measurements on the molecule ThO [2], which shows that experiments are currently in the midst of eliminating proposed extensions to the Standard Model.

The electron EDM is of interest because it is a P-odd, T-odd effect, making room for PV in an extended Standard Model. To see why an EDM would have this property, we consider a generic charged, spin 1/2 particle in the presence of an electric and magnetic field. This

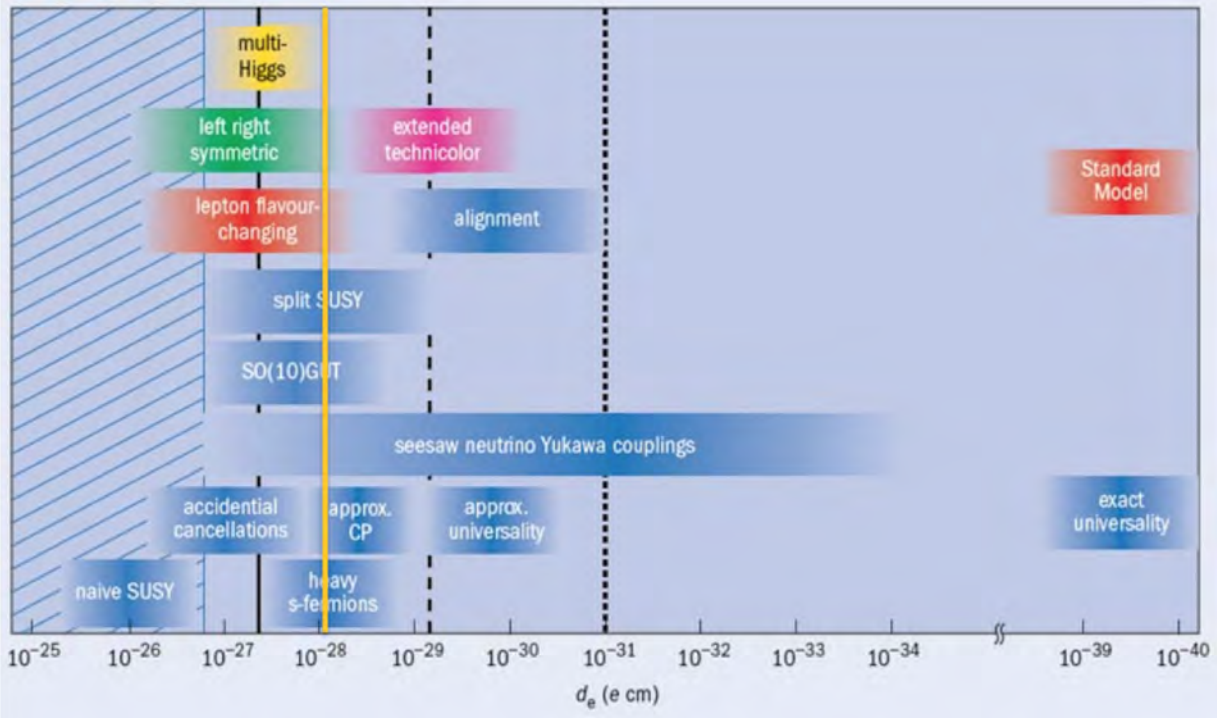

Figure 1: Predictions for the eEDM by various extensions to the Standard Model. The current upper limit from the 2014 ThO result is given by the yellow line. Dashed lines represent estimates for future sensitivity of current experiments, showing how we can constrain potential extensions by improving the experimental upper limit. Adapted from [3].

particle would have the interaction Hamiltonian

$$\mathcal{H} = -\boldsymbol{\mu} \cdot \mathbf{B} - \mathbf{d} \cdot \mathbf{E}, \tag{1.1}$$

where $-\boldsymbol{\mu} \cdot \mathbf{B}$ is the interaction of the magnetic dipole moment with the magnetic field and $-\mathbf{d} \cdot \mathbf{E}$ is the interaction of the EDM with the electric field. The symmetry transformations of these terms are given in Table 1. From this table, it is clear that the magnetic interaction term will always be even under any of the transformations. However, the interaction of the electric dipole moment and the electric field will be antisymmetric under both parity and time reversals [4]. Figure 2 gives a graphical representation of P and T violation in a charged spin 1/2 particle. Notice that this argument should in principle apply to any charged particle, not just the electron. Indeed, there are predictions for proton, neutron, and quark EDMs. Experimentally constraining the EDM values of various fundamental particles provides valuable insight into Standard Model extensions, while an actual observation of any EDM would shape all future theoretical work on high energy particle physics.

	B	μ	E	d
P	+	+	-	+
C	-	-	-	-
T	-	-	+	-

Table 1: The symmetry transformation properties of each term in equation 1.1. Adapted from [4].

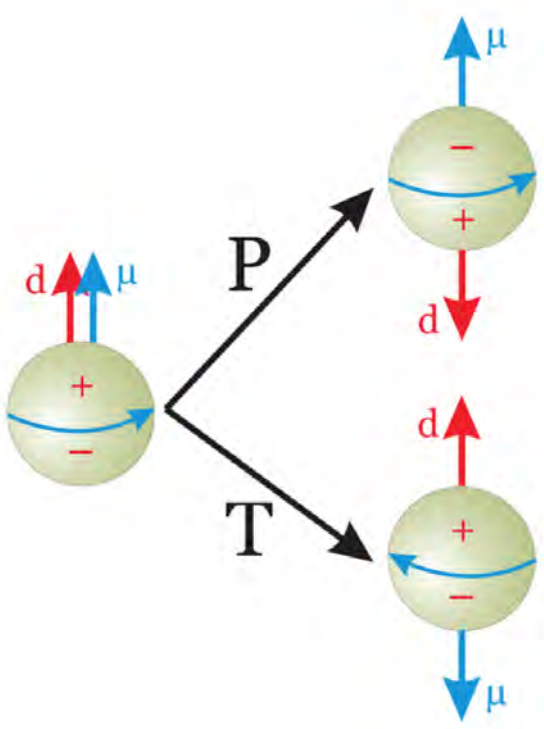

Figure 2: The EDM of a generic spin 1/2 charged particle. From [5].

1.2 Interest in PbF

The easiest way to test for an electron electric dipole moment would be to observe a free electron's behavior in an electric field. Of course, an electron is a charged particle, so it would quickly accelerate out of the experiment under these circumstances. The best way to circumvent this problem is to observe what happens to an unpaired electron in an atom or molecule in the presence of an electric field, where the observed effect is assumed to be the result of the electron EDM.

In order to circumvent Schiff's theorem, which states that the average force on each charged particle in an atom must be zero, the atoms or molecules selected for such an experiment must put the electron into a relativistic environment. Additionally, the attainable

effective electric field in certain polar molecules is higher than the equivalent effect in atoms. Indeed, molecules allow for a more varied selection of features useful for a wide variety of experiments [6]. Most systems of interest for eEDM experiments are built out of heavy nuclei and selected for features such as strong internal effective electric fields [7].

This thesis focuses on the particular molecule lead fluoride (PbF), a candidate molecule for eEDM detection for many of the reasons outlined above, including a heavy nucleus and a large internal electric field. It also boasts a small sensitivity to external magnetic fields, characterized by the molecular g-factor ($g \approx 0.04$). Although the PbF molecule is intrinsically less sensitive to eEDM effects than the ThO system since it has a smaller internal electric field, it has the advantage of an eEDM sensitive ground state [8], which would allow for longer measurements to reduce noise. ThO, on the other hand, must first be excited and has a state lifetime-limited measurement window. Like ThO, ^{207}PbF has a pair of low-lying, opposite parity states that display coincidental near-degeneracy [9], which can be seen in Figure 3. This near-degeneracy is a useful quality that allows for the reduction of many systematic errors in an eEDM experiment.

There have been several theoretical studies of PbF to assess its potential for experiments probing both P-odd, T-odd effects (such as the eEDM) and P-odd, T-even effects [10], [9]. Although not the focus of this thesis, P-odd, T-even effects are also of interest to the atomic and molecular physics community, as they are another instance of parity violating processes that could represent New Physics. One such effect, representative of current circulation in the nucleus, has previously been observed in atomic cesium by Wieman, *et al.* [11], but its verification through another system would be another valuable application of PbF. Theoretical study of PbF has recently picked up steam, due to the resolution of difficulties in analyzing PbF spectra and discovery of the near-degeneracy of opposite parity states in ^{207}PbF [12], [9].

The theoretical development in the study of PbF has spurred spectroscopic experiments on the molecule in recent years to guide and verify theoretical predictions. An optical Fourier transform setup has given a firm foundation for analysis of fine-structure interaction parameters [14], while microwave Fourier transform spectroscopy has allowed for precision determination of hyperfine parameters in various stable isotopes of PbF, [13], [15], [16], [17]. Further work on PbF has been performed on the Zeeman splitting behavior of the molecule. To investigate the near cancellation in the $\Lambda + g_s\Sigma$ term in the expression for the molecular g-factor g_J, Alexander Baum '11's senior thesis concentrated on a thorough analysis of Zeeman splitting in the ground state of PbF [5]. While a good understanding of the internal structure of a molecule is important for designing an eEDM experiment, precise understanding of the effects of stray magnetic fields and other systematic errors is an important factor in converting an experimental measurement into an upper limit of the

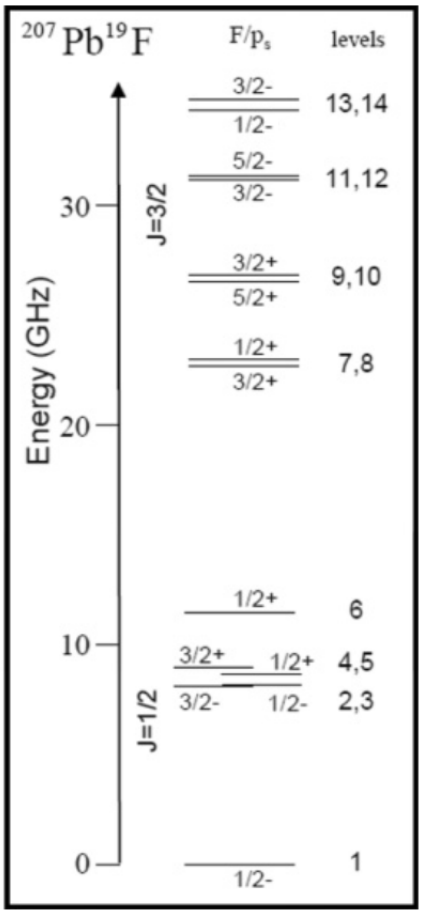

Figure 3: The hyperfine energy levels of the $v = 0$ ground state of ^{207}PbF. Note the accidental degeneracy of states of opposite parity in the cluster of levels 2-5. From [13].

eEDM.

PbF boasts a wide body of existing literature that serves as an appealing foundation for an eEDM experiment. The main goal of this thesis is to leverage the abundance of existing datasets, which describe multiple isotopes and vibrational levels of the molecule, and provide one detailed, global fit of spectroscopic parameters for the molecule. This global fitting will be accomplished using the Dunham potential formulation, which assumes a strict isotopic and vibrational scaling for the parameters which describe a molecule's energy structure [18], [19]. The well-understood isotopic mass scaling of this fitting procedure allows for a robust analysis of diatomic molecules, which has been carried out for several species, including an analysis of O_2 [20], HF [19], and YbF by Zachary Glassman '14 , [21], [22].

Although such a global fit is useful for a much more detailed description of a molecule for applications such as an eEDM experiment, it has more direct applications in predicting spectral features of the molecule for further spectroscopic experiments. In the case of PbF, ^{205}PbF is an isotopologue of interest because it has a nonzero nuclear quadrupole moment

(NQM) term, which could further displace states of opposite parity to be more degenerate than the ^{207}PbF case. However, ^{205}Pb is a long-lived radioactive isotope, presenting some experimental complications. Hence another goal of this thesis is to use the global fit of existing PbF data predictively to evaluate whether spectroscopic analysis of ^{205}PbF is worth pursuing. This predictive work demonstrates the power of the global Dunham fitting procedure, and should strengthen PbF as a viable candidate for further eEDM and related parity violation research.

2 Electric Dipole Moment Theory

Rather than being a complete treatment of electric dipole moments in the Standard Model, this chapter is intended to provide motivation for the existence and suspected magnitudes of various EDM terms of interest in the physics community, and to provide thorough background for the features of PbF as a molecular system in relation to existing eEDM experiments. Additionally, the aim of the theoretical discussion in this chapter is to provide a useful entryway into exploring more detailed literature on the subject of EDM behavior in the Standard Model and the molecular experiments seeking to measure various EDM terms.

2.1 The Electron Electric Dipole Moment

We provided a plausibility argument for the existence of an eEDM in Chapter 1 of this thesis. At a more fundamental level, these claims are supported by Feynman diagram-level calculations. Since Feynman diagrams are graphical representations of terms in a series expansion of interaction cross-sections, they hold valuable information about the expected magnitude of the interactions and effects they describe (see [23] for an introduction to Standard Model calculations). In the following section we will extend our discussion by providing an overview of Standard Model predictions for the eEDM, explaining how an eEDM can be measured in a molecular system, and reviewing several current experiments attempting to carry out such a measurement.

2.1.1 Theoretical Predictions

This section's discussion of the eEDM in the Standard Model follows the approach of Commins and DeMille [7]. The main mechanisms for the existence of the electron electric electric dipole moment are radiative corrections to electromagnetic interactions in the form weak interactions, which are also CP-violating. See Chapter 1 for a disucssion of the fundamental symmetries. These mechanisms provide the same kind of asymmetries as the simpler model discussed in Figure 2, in which the eEDM does not behave identically under time reversal or P reversal.

CP violation is accommodated in the Standard Model through the 3×3 Cabibbo-Kobayashi-Maskawa (CKM) matrix, which allows for the coupling of different quark generations to one another and describes the amount of CP violation allowed through these couplings with a single parameter, δ. This matrix essentially rotates a physical quark state slightly into a so-called Cabibbo-rotated state, which is made of a superposition of primarily the same generation of quark and a small additional factor of quarks in the other generations. In a weak-interaction process, the W-bosons couple to the Cabibbo-rotated states rather than

the physical states, so that a small number of processes actually change quark generations and violate CP invariance. The CKM matrix is defined by four empirical parameters—the generalized Cabibbo rotation angles, θ_{12}, θ_{23}, θ_{23}, and the aforementioned CP violating phase factor, δ. The value of δ has been empirically established through measurements of CP violation in K- and B-mesons [23]. Although this value is actually quite large, the amount of CP violation allowed by the Standard Model is suppressed by the very small amount of quark mixing that occurs; in other words, the small values of θ_{12}, θ_{23}, θ_{23} limit the amount of CP violation explained by the CKM matrix [7]. Since we know the Standard Model does not explain the CP violation required for the matter-antimatter imbalance in the universe, and all observed instances of CP violation can be explained with the δ phase factor [23], we suspect there are other sources of CP violation independent of the CKM matrix.

To calculate the value of the eEDM, d_e, predicted by the Standard Model, we sum over the contributions of Feynman diagrams of increasing complexity (and, thus, decreasing contribution). The eEDM arises from coupling virtual quarks to virtual W-bosons, which requires at least two loops. However, we see in Figure 4 that the two-loop diagram has a net contribution of zero to d_e, since the symmetry of the loop ensures that any contribution from the coupling at vertex v is cancelled out by the complex conjugate contribution from vertex v'. Summing over all three-loop diagrams similarly yields a net contribution of zero. The first order of Feynman diagram that does not cancel in this calculation is the four-loop level, which, along with the relatively small levels of CP violation predicted by the Standard Model through the CKM matrix, yields a prediction of $d_e < 10^{-38}$ e·cm.

Virtually every extension to the Standard Model predicts the existence of new particles which would allow for an eEDM contribution through a lower order diagram, which is why almost all such extensions predict larger values for the eEDM. For example, consider the case of a generic Standard Model extension which allows an unknown virtual particle, X, to couple via another CP-violating phase, ϕ, and coupling factors f. The diagram in Figure 5 shows such a hypothetical extension that enables a one-loop contribution to d_e. Actual extensions that exhibit this behavior, among others, are the supersymmetry (SUSY) theories. Depending on the assumptions about the values of ϕ (of similar magnitude to δ is a crude estimate) and the mass of X, a rough estimate for d_e as predicted by extensions to the Standard Model places the eEDM magnitude in the range 10^{-26} e·cm $< d_e < 10^{-24}$ e·cm. Other extensions predict values all the way down to 10^{-31} e·cm; see Figure 1 for experimental values and predicted ranges. Placed in the context of the current experimental upper limit on the value of the eEDM magnitude, $d_e < 8.7 \times 10^{-29}$ e·cm, we see that experimental approaches are certainly in the midst of placing constraints on extensions to the Standard Model.

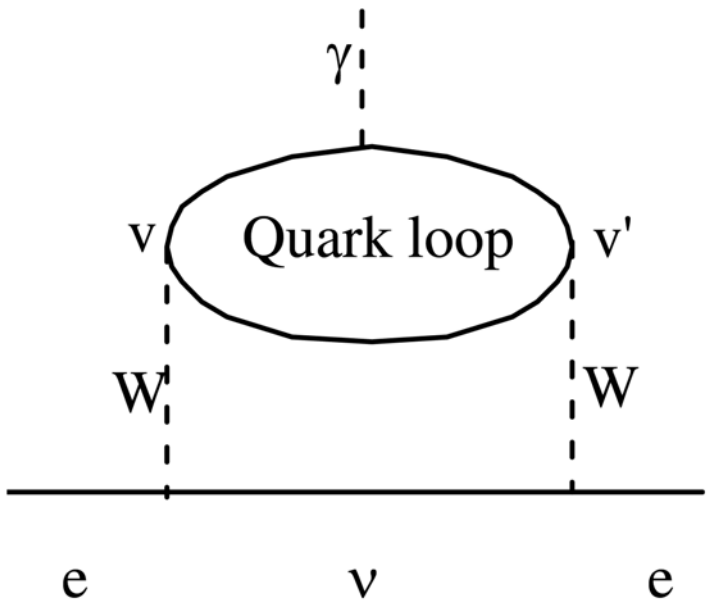

Figure 4: The Standard Model two-loop diagram for the eEDM arising from coupling to virtual quarks via virtual W-bosons. Note that any contribution from the CKM matrix at vertex v is canceled out by the corresponding contribution from vertex v'. From [7].

2.1.2 Measuring the Electron EDM

Conceptually, the measurement of an eEDM corresponds to measuring the change in precession frequency of an electron with associated changes in the electric field it is in. Given an electron polarized so that its spin is perpendicular to parallel electric and magnetic fields, we can measure the precession frequency of the spin due to these fields. Subsequently reversing the sign of the electric field results in an overall change in the spin precession since the eEDM contribution will take the opposite sign. Since the magnetic moment is much larger than the electric dipole moment, the spin precession will change some small amount in frequency, rather than change in an unpredictable way. The difference in precession frequencies between these two configurations, then, corresponds to the magnitude the eEDM [24].

To describe this experimental approach using atoms or molecules in more detail, we again follow Commins and DeMille [7]. Most experimental searches for the eEDM follow a similar process, for which we can develop a toy model. Consider a system of an atom and an unpaired electron of total spin $\frac{1}{2}$ with enhancement factor R, which corresponds to the system's eEDM sensitivity. Incidentally, this unpaired electron makes the atom paramagnetic, since the unpaired electron tends to align against external magnetic fields [25]. In eEDM literature, paramagnetism is shorthand for the presence of an unpaired electron; without the unpaired electron in the system, the eEDM effects of paired electrons tend to cancel out.

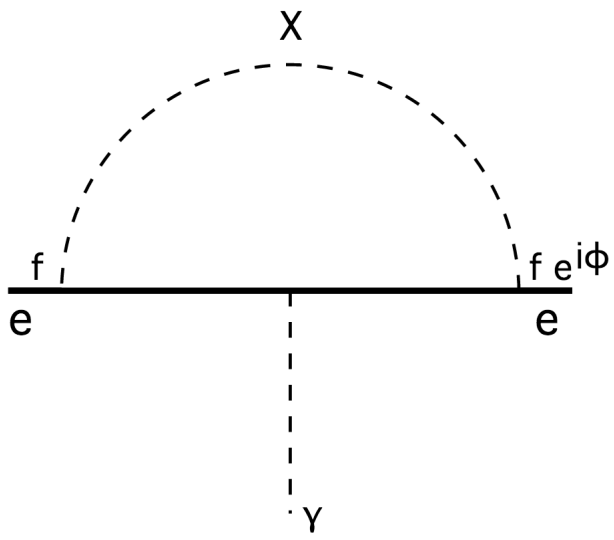

Figure 5: The one-loop diagram giving rise to an eEDM in an unspecified extension to the Standard Model. New terms are an unknown virtual particle X, another CP-violating phase, ϕ, and new couplings f. Note the asymmetry of the loop provided by the phase ϕ, which no longer ensures cancellation of verteces as is the case in the Standard Model. From [7].

Suppose the atom is initially in the state

$$\psi_0 = \frac{1}{\sqrt{2}}\begin{pmatrix}1\\1\end{pmatrix}, \tag{2.1}$$

which corresponds to a spin aligned with the x-axis, and that the external electric ($\mathbf{E}$) and magnetic ($\boldsymbol{B}$) fields are aligned with the z-axis. If we let the spin evolve with time, the spin precesses through an angle

$$\vartheta = \frac{-(d_e RE - g_s \mu_B B/2)\tau}{2\hbar}, \tag{2.2}$$

where d_e is the eEDM magnitude, $-g\mu_B/2$ is the spin magnetic moment of the unpaired electron, and τ is the elapsed time. Therefore, the new quantum state of the system after time τ is

$$\psi = \frac{1}{\sqrt{2}}\begin{pmatrix}e^{-i\vartheta}\\e^{i\vartheta}\end{pmatrix}. \tag{2.3}$$

The next steps in our model experiment are to prepare an analyzer state, and then use a detector to read out the final result. In this case, the analyzer matrix

$$A = \frac{1}{\sqrt{2}}\begin{bmatrix}1 & 1\\-i & i\end{bmatrix} \tag{2.4}$$

can be thought of as the process of collapsing the wavefunction into an observable state, which results in the detection state

$$\psi' = \begin{pmatrix}\cos\vartheta\\\sin\vartheta\end{pmatrix}. \tag{2.5}$$

Supposing the detector yields the probability of finding the upper component of Equation 2.5, the result of measuring a beam of N atoms (assuming 100% detection efficiency) is

$$S = N \cos^2 \vartheta. \tag{2.6}$$

Finally, note that of the two components of Equation 2.2,

$$\frac{d_e RE}{2\hbar} \ll \frac{g_s \mu_B B/2}{2\hbar}. \tag{2.7}$$

To isolate the term that contains the eEDM term, we measure the precession when $\mathbf{E}$ and $\mathbf{B}$ are parallel and antiparallel, since the relative signs of the terms in ϑ reverse under these conditions. The precession contribution of spin magnetic moment is well-understood, so this known quantity and the small-angle approximation combine to isolate the eEDM contribution to the signal by taking a difference of the two measurements.

It can be further shown that the noise in a measurement of d_e follows the form

$$\delta d_e = \sqrt{\frac{(\delta\vartheta^{mag})^2 + \frac{1}{N_0}}{t\tau_0}} \left| \frac{\hbar}{\mathbf{E_{eff}}} \right|, \tag{2.8}$$

where N_0 is the number of particles in the shot, $\delta\vartheta^{mag}$ is the magnetic fluctuation contribution, t is the total observation time of the experiment which is repeated t/τ_0 times, and $\mathbf{E_{eff}}$ is the effective field acting on the electron inside the molecule. Thus, it is not possible to decrease the noise in the experiment after a certain point by only increasing the number of particles per shot, since magnetic noise will eventually dominate. With careful shielding of magnetic fields and selection of materials which will reduce stray currents and magnetic fluctuations, this magnetic fluctuation error is predicted not to be significant at the current level of eEDM sensitivity.

In addition to noise, precision measurements of the eEDM are sensitive to systematic errors. For such measurements, P-odd, T-odd effects are interpreted in terms of the eEDM. However, there are other P-odd, T-odd effects that can add systematic error to a measurement. For example, a dependence of $\mathbf{B}$ on the sign of $\mathbf{E}$ through various mechanisms is indistinguishable from an eEDM effect without further experimental design. Some of these effects include leakage currents between electric field-generating electrodes, the contribution of a motional magnetic field term in beam experiments, and the contribution of a geometric phase to the precession experiment. On the other hand, the careful selection of a molecule can mitigate both the noise and systematic error contributions to the eEDM measurement, making the search for viable molecular systems a key element of the overall effort to observe the eEDM.

2.1.3 Ongoing Experiments

There are currently several different molecules being investigated for the purpose of eEDM experiments, including the to-date most sensitive test molecule, ThO [2], from which the established upper limit of $d_e < 8.7 \times 10^{-29}$ e·cm has been derived. Other prominent molecules under investigation are YbF [26], which held the previous upper limit, and HfF^+ [27]. Each of these molecules provides its own approach and advantages to the measurement process, but all focus on minimizing systematic errors and key terms in the noise expression given by Equation 2.8.

YbF was the first molecular system that produced a measurement of the eEDM that held the upper limit. This measurement was released in 2011, beating the previous record-holding experiment on atomic thallium [26]. The YbF molecule has two key traits that allowed for a significant improvement of the eEDM upper limit. First, the internal electric field inside the molecule is much larger under external polarization than laboratory-generated fields can be, which clearly reduces the magnitude of the error given by Equation 2.8. Additionally, the molecule can be strongly polarized to greatly reduce motional magnetic field errors [28]. Developments on the experiment between 2002 and 2011 allowed for a reduction in other systematic errors, such as nonuniform electric fields and shifting magnetic fields within the apparatus [26].

An improvement on the YbF measurement was achieved in 2014 using ThO. As previously mentioned, this molecule has provided the most sensitive measurement to date, again thanks to molecular properties which reduce noise and the effect of systematic errors [2]. The Advanced Cold Molecule eEDM experiment focused on the $^3\Delta_1$ state of ThO, which can be polarized with a laboratory electric field, allowing the measurement to take advantage of one of the largest internal electric fields found in diatomic molecules. This particular state also has a long lifetime, allowing for good integration time in the measurement, again reducing the error as given in Equation 2.8. Furthermore, the $^3\Delta_1$ state of ThO boasts a very small g-factor, which quantifies the molecule's magnetic moment and, thus, response to stray magnetic fields, on the order of 0.01 to 0.1. Finally, a particularly luminous cryogenic molecular beam source allows for more efficient shot counts through flux and detection improvements. Perhaps the most useful aspect of the $^3\Delta_1$ state is its Ω-doubling, which produces two states of opposite parity. Effectively, these states allow for the spectroscopic reversing of the effective electric field that the electron reacts to, which eliminates the need to reverse the laboratory field. This approach, in turn, minimizes many of the systematic effects discussed in the previous section [1].

Another proposed approach to measuring the eEDM with molecules is to trap ionic molecules and perform precision spectroscopy that takes advantage of their trapped state [29]. Recent efforts have focused on the ions HfF^+ and, in the future, ThF^+ [27], [30]. Both

of these molecules boast the same $^3\Delta_1$ state that made the ThO experiment successful, and can therefore also take advantage of Ω-doubling to reduce systematic errors. Additionally, ionic trapping should allow for a much longer integration time to further reduce noise.

An important part of each of these experiments is a precise understanding of the internal structure of their respective molecules. This understanding is achieved through precision spectroscopy experiments, which give a detailed description through fine-structure and hyperfine parameters. The only way to detect a minuscule effect such as an eEDM despite the presence of these much larger effects is to understand them as completely as possible through high precision spectroscopy.

2.2 Electric Dipole Moments of Other Fundamental Particles

Figure 2 provides justification for the existence of an EDM of a generic spin-1/2 charged particle. Although we have been concerned mostly with the eEDM so far in this chapter, we should suspect that other fundamental particles also have EDMs. Indeed, it is possible to write down EDM contribution diagrams for quarks in the Standard Model, as in Figure 6. Since hadrons like neutrons and protons are made up of quarks, we might also suspect that these particles have EDM terms that change between the Standard Model and various extensions. In fact, the nEDM is another highly sought-after measurement to provide insight into physics beyond the Standard Model. In this section, we will discuss a brief overview of nEDM experiments, and discuss a recently proposed molecular experiment that could place better limits on various hadronic and quark EDM terms.

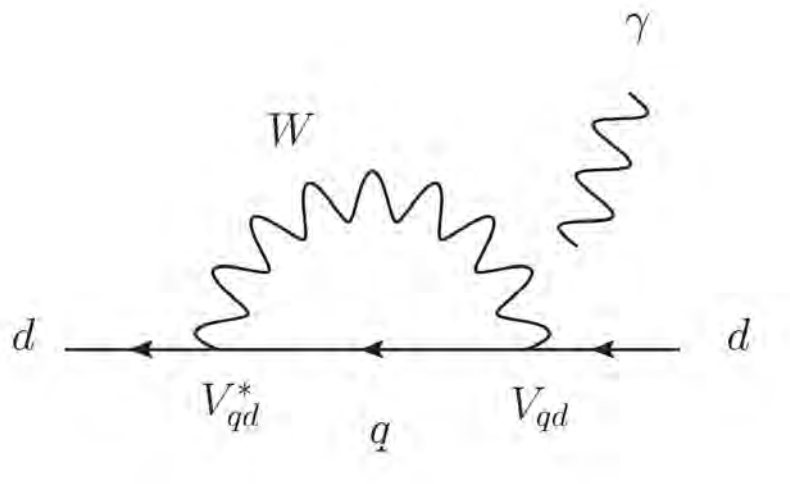

Figure 6: One-loop diagram contributing to the d-quark EDM in the Standard Model. V_{qd} is an entry of the CKM matrix. From [31].

2.2.1 Neutron Electric Dipole Moments

It might seem strange to talk about a neutron electric dipole moment, since neutrons are neutral particles. However, if we consider the fact that neutrons are made of three constituent quarks, two of which have the same charge, it makes some more intuitive sense to suspect there to be a charge separation in the form of an nEDM. The Standard Model does predict a value for the nEDM, to which the diagram in Figure 7 contributes. Like the eEDM, the magnitude of the nEDM is much smaller in the Standard Model than in virtually every extension. Therefore, the neutron EDM also provides a promising avenue for placing constraints on extensions to the Standard Model. The two quantities are complementary; a measurement of the nEDM would not necessarily improve our ability to predict the eEDM [24].

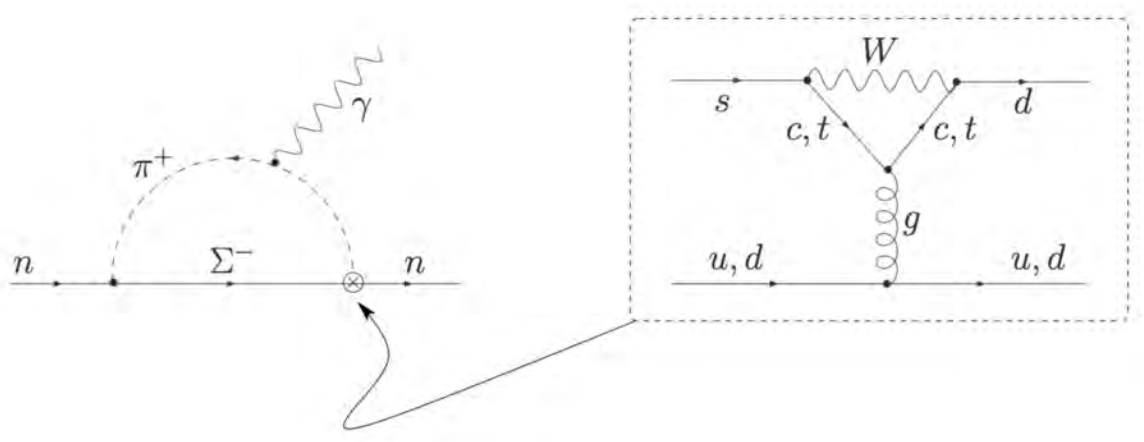

Figure 7: A single diagram contributing to the neutron EDM in the Standard Model. From [32].

The current nEDM upper limit was established by the experiment at the Institut Laue-Langevin in Grenoble in 2006 using trapped ultracold neutrons. This upper limit was placed at a value of $d_n < 2.9 \times 10^{-26}$ e·cm [33], while the Standard Model calculation yields a value of $d_e \sim 10^{-31}$ e·cm [34]. Trapped neutron experiments are conceptually very similar to the approach taken in molecular eEDM experiments; the neutrons are subjected to parallel and antiparallel electric and magnetic fields, and their precession frequency is measured in these two configurations. A change in precession frequency would signal the contribution of the nEDM [24]. Naturally, these experiments suffer from similar systematic errors to molecular eEDM experiments, as well. Motional magnetic field contributions and magnetic field fluctuations contribute to geometric phase differences that hide the nEDM contribution, so controlling and understanding the magnetic field inside the apparatus is crucial in improving the sensitivity of the experiment [34].

Future efforts on reducing the upper limit on the nEDM have been focused on the cold

neutron trapping approach. With more sensitive comagnetometer atoms, providing better information on fluctuations in the apparatus magnetic field and more efficient methods of generating cold neutrons, the sensitivity of measurements such as the current Oak Ridge experiment will continue to improve [24]. As the value of the nEDM is more tightly constrained constrained, further restraints will result on extensions to the Standard Model.

2.2.2 Leveraging the Magnetic Quadrupole Moment

In our previous discussions of spin precession measurements, we assumed that the only P-odd, T-odd contribution was caused by the existence of an eEDM. This assumption neglects P-odd, T-odd contributions from other sources, which are the nuclear Schiff moment and the nuclear magnetic quadrupole moment (MQM). The effective Hamiltonian for a paramagnetic diatomic molecule is therefore more completely described by

$$\boldsymbol{H}_{eff} = W_d d_e \boldsymbol{S}\cdot\boldsymbol{n} + W_Q \frac{Q}{I}\boldsymbol{I}\cdot\boldsymbol{n} - \frac{W_M M}{2I(2I-1)}\boldsymbol{S}\hat{\boldsymbol{T}}\boldsymbol{n}, \tag{2.9}$$

where $\boldsymbol{n}$ is a unit vector defining the molecular axis, $\boldsymbol{I}$ is the nuclear spin, $\boldsymbol{S}$ is the effective electronic spin, d_e is the magnitude of the eEDM, Q is the nuclear Schiff moment, $M\hat{\boldsymbol{T}}$ is a tensor describing the MQM, and W_d, W_Q, and W_M are calculated parameters for a given molecular system. Both of these previously neglected effects result from electron-nucleon interactions, so they can shed light on nucleon EDM terms such as proton, neutron, and quark EDMs [35].

The Schiff theorem states that the EDM of the nucleus is screened by electrons, so it has been difficult to leverage the Schiff moment for any sort of hadronic or nuclear EDM measurement. For this reason, the effect is negligible in most molecules compared to the eEDM contribution. However, it has been shown that the MQM provides a much larger effect resulting from electron-nucleon interactions, since Schiff's theorem does not screen magnetic interactions [35]. Therefore, it is in principle possible to measure the P-odd, T-odd spin precession of a molecule with a large MQM and produce limits on the combined MQM and eEDM contributions. These contributions can then be teased apart based on molecular electronic structure calculations [36], [37]. The proton, neutron, and quark EDM terms correspond to the MQM in a known way, so a sensitivie MQM measurement would provide tighter constraints on the magnitudes of these terms [35].

Experimentally, the process of measuring a P-odd, T-odd spin precession to obtain an MQM measurement does not differ much from previous eEDM spin precession measurements. ThO, the same molecule as the eEDM measurement, is a potential candidate for an MQM measurement, assuming further developments in the sensitivity of the experiment [38]. However, it has recently been discovered that TaN would also be a good candidate molecule for such a measurement, since it has a low-lying $^3\Delta_1$ state that provides the same

systematic error control as the ThO experiment, as well as a highly deformed nucleus that gives rise to a large MQM. Additionally, the $^3\Delta_1$ in TaN is suspected to be longer lived than ThO's equivalent state, making a spin-precession measurement in TaN more sensitive than the recent ThO eEDM measurement due to the possibility of longer integration times [35], [36]. Many of these calculations and predictions have yet to be experimentally verified, providing a strong motivation for spectroscopic analysis of the TaN molecule, some of which has previously been performed [39], [40], [41].

3 Spectroscopic Structure of PbF

The discussions in this chapter assume an understanding of the theory of diatomic molecules at the level of Gordy & Cook [42]. A similar level of theoretical overview was also provided in Zachary Glassman '14's senior thesis [21].

As discussed in Chapter 1, understanding the spectroscopic structure of candidate molecules is highly important in quantifying systematic errors and uncertainties in EDM experiments and, ultimately, in producing a value for the measurement. Producing a value for the upper limit on an eEDM experiment is particularly sensitive to the expectation value of the electric field at the nucleus. Generally, this value is theoretically calculated, but it is possible to produce experimental checks on these calculations with precision spectroscopy via the electric field gradient at the nucleus, q, the Fermi contact parameter, b_F, and other parameters that describe electron behavior near the nucleus. While it is not possible to measure the electric field directly, these parameters do indirectly validate our understanding of its value and the accuracy of the wavefunctions used in the calculation. To illuminate the role of q in precision spectroscopy and the structure of PbF, we will begin our discussion with previous work on YbF.

3.1 YbF

Between 2011 and 2014, ^{174}YbF held the most sensitive upper limit on the eEDM [26]. While YbF has several stable isotopologues (including ^{170}YbF, ^{171}YbF, ^{172}YbF, ^{173}YbF, ^{174}YbF, and ^{176}YbF), ^{174}YbF is the most abundant and has a relatively uncomplicated spectrum. As described in Chapter 2, the ^{174}YbF measurement was superseded by ThO thanks in part to the near-degeneracy of states of opposite parity [2]. These states allow for the spectroscopic reversal of the electric field in the experiment, which is significantly less sensitive to systematics compared the manual reversal.

The other even isotopes of Yb do not promise significant departures from the ^{174}YbF energy structure, since the identical spin structure of these isotopologues does not produce extra couplings. The odd isotopologues of YbF, however, boast nonzero nuclear spins that perturb the energy structure of the molecule. This behavior highlights a common trend; often it is necessary to analyze the spectra of the simplest isotopologues first, using those results as a base for which to analyze isotopologues with further spin couplings. For example, in the YbF analysis given in Zachary Glassman '14's senior thesis, the effective Hamiltonian used to analyze the ground state (and ground vibrational state) of the even isotopologues is [21]

$$^{\text{eff}}\mathbf{H}^{X^2\Sigma^+}_{\text{even}} = B\mathbf{N}^2 - D(\mathbf{N}^2)^2 + \gamma\mathbf{N}\cdot\mathbf{S} + b_F(\text{F})\mathbf{I}\cdot\mathbf{S} + c(\text{F})\left(I_z S_z - \frac{1}{3}\mathbf{I}\cdot\mathbf{S}\right). \tag{3.1}$$

The simpler of the two odd isotopologues in this case is ^{171}YbF, since it has a nuclear spin and parity of $\frac{1}{2}-$ [43]. This spin necessitates additional hyperfine parameters due to the interaction of the nonzero nuclear spin of the Yb atom in the molecule with other spins. These extra terms appear on the second line below in the effective Hamiltonian for ^{171}YbF [21]:

$$\begin{aligned}{}^{\text{eff}}\mathbf{H}^{X^2\Sigma}_{171} = B\mathbf{N}^2 - D(\mathbf{N}^2)^2 + \gamma\mathbf{N}\cdot\mathbf{S} + b_F(\mathrm{F})\mathbf{I}^{(\mathrm{F})}\cdot\mathbf{S} + c(\mathrm{F})\left(I_z^{(\mathrm{F})}S_z - \frac{1}{3}\mathbf{I}^{(\mathrm{F})}\cdot\mathbf{S}\right) \\ + b_F(\mathrm{Yb})\mathbf{I}^{(\mathrm{Yb})}\cdot\mathbf{S} + c(\mathrm{Yb})\left(I_z^{(\mathrm{Yb})}S_z - \frac{1}{3}\mathbf{I}^{(\mathrm{Yb})}\cdot\mathbf{S}\right). \end{aligned} \tag{3.2}$$

Analysis of the ^{171}YbF isotopologue hyperfine structure has recently been performed using optical and microwave spectra [22].

So far no completely successful analysis exists for the hyperfine structure of ^{173}YbF. Attempts at analyses have been held up by the complicated structure of the spectra for this isotopologue, which Glassman attempted to analyze using the effective Hamiltonian [21]

$$\begin{aligned}{}^{\text{eff}}\mathbf{H}^{X^2\Sigma}_{173} = B\mathbf{N}^2 - D(\mathbf{N}^2)^2 + \gamma\mathbf{N}\cdot\mathbf{S} + b_F(\mathrm{F})\mathbf{I}^{(\mathrm{F})}\cdot\mathbf{S} + c(\mathrm{F})\left(I_z^{(\mathrm{F})}S_z - \frac{1}{3}\mathbf{I}^{(\mathrm{F})}\cdot\mathbf{S}\right) \\ + b_F(\mathrm{Yb})\mathbf{I}^{(\mathrm{Yb})}\cdot\mathbf{S} + c(\mathrm{Yb})\left(I_z^{(\mathrm{Yb})}S_z - \frac{1}{3}\mathbf{I}^{(\mathrm{Yb})}\cdot\mathbf{S}\right) \\ + eQq(\mathrm{Yb})\frac{3I_z^{(\mathrm{Yb})} - \left(\mathbf{I}^{(\mathrm{Yb})}\right)^2}{4I^{(\mathrm{Yb})}\left(2I^{(\mathrm{Yb})}-1\right)}. \end{aligned} \tag{3.3}$$

These complications arise from two main factors. First, the $\frac{5}{2}-$ spin of the ^{173}Yb nucleus [43] enables more combinations than the ^{171}Yb isotope, as can be seen in Figure 8. This results in many more transitions to observe and a much denser spectrum, which can be difficult to assign correctly. Additionally, any nucleus with more than two spin states (in other words, with nuclear spin $I > \frac{1}{2}$) has an electric quadrupole moment, which results in the eQq term in Equation 3.3. This electric hyperfine term can be quite large and therefore can significantly change the structure of a spectrum relative to simpler cases where it is not present.

3.1.1 The Nuclear Electric Quadrupole Moment and the eQq

The eQq is the product of the electron charge, e, the electric quadrupole moment of the nucleus, Q, and the electric field gradient at the nucleus q (also sometimes referred to as EFG [45]). Thus, this parameter provides experimental means to evaluate the theoretically calculated EFG that is related to the effective electric field calculation crucial in evaluating the value of an EDM measurement. Although not all molecules used for EDM experiments

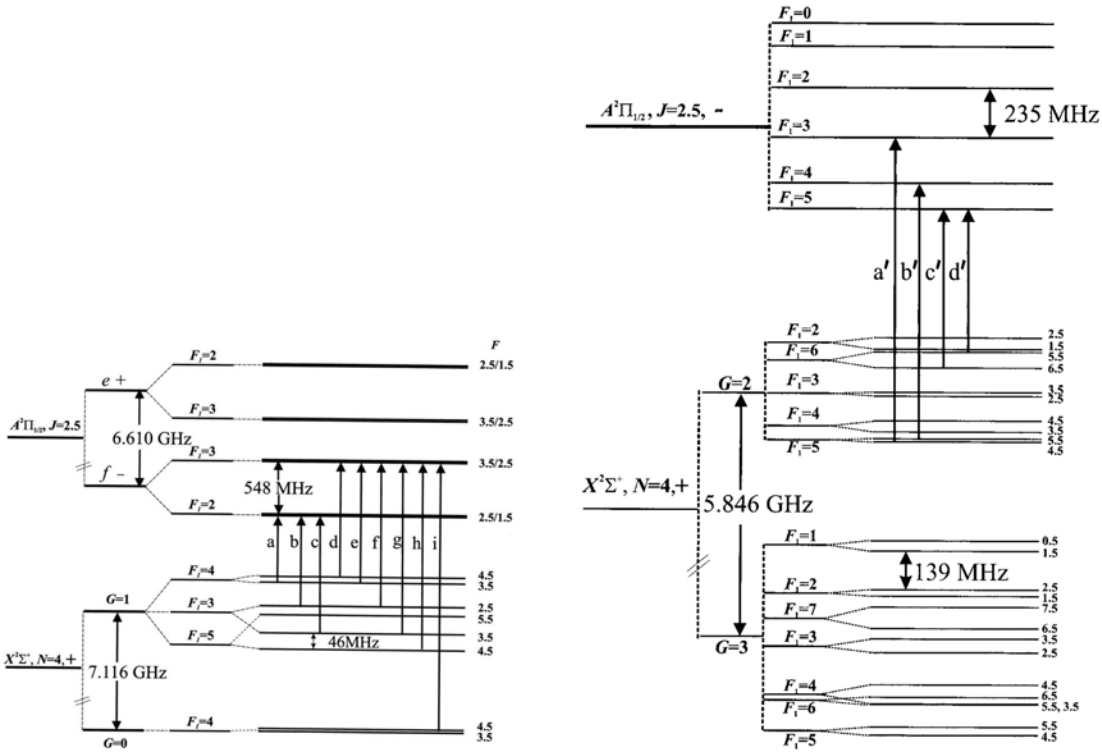

(a) ^{171}YbF (b) ^{173}YbF

Figure 8: Energy level diagrams for two odd isotopes of YbF with nonzero Yb nuclear spin. The number of energy levels in ^{173}YbF is much larger than in ^{171}YbF due to the $\frac{5}{2}-$ spin nucleus of ^{173}Yb contributing more spin states to the system. From [44].

have an isotopologue with an eQq parameter, resolving it for several different molecules that can also be theoretically treated provides a reliable method for testing the procedures used to produce a value for the EFG, and thus the effective electric field as well. Additionally, the eQq provides an extra parameter to perturb energy levels present in analogous systems, such as those that are known to be eEDM sensitive in ^{207}PbF. The eQq could push these states to even closer near-degeneracy, so the spin $\frac{5}{2}-$ ^{205}PbF is a system worth investigating predictively, if not experimentally.

3.2 PbF

The purpose in analyzing PbF in this thesis is twofold. First, a global fit across isotopologues will provide the most complete and robust model of the molecule to date. Should PbF be used as the system for a precision measurement experiment (see applications subsection below), this global fit is essential in limiting systematic errors. Second, this framework will allow us to predictively explore ^{205}PbF using a theoretically calculated value of the eQq. This

analysis will give us an initial sense of how promising this particular isotopologue of PbF is as a candidate for experiments searching for the eEDM, parity violating nuclear anapole, and change in the fundamental constants and whether further spectroscopic work should be pursued in light of ^{205}PbF's relative rarity and minor radioactivity.

3.2.1 Structure of PbF

Table 2: PbF Isotope Information [46], [43], [47]

Isotope	Atomic mass (u)	Abundance (%)	Nuclear Spin	Magnetic moment (g_N)	Quadrupole moment (fm^2)
^{19}F	18.998 403 22(7)	100	1/2+	+2.628 868(8)	
^{204}Pb	203.973 043 6(13)	1.4(1)	0+	0	
^{205}Pb	204.974 481 8(13)		5/2−	+0.711 7(4)	+23(4)
^{206}Pb	205.974 465 3(13)	24.1(1)	0+	0	
^{207}Pb	206.975 896 9(13)	22.1(1)	1/2−	+0.592 583(9)	
^{208}Pb	207.976 652 1(13)	52.4(1)	0+	0	

Structurally, PbF shares many similarities with YbF. Both are open-shell molecules, meaning they have an unpaired electron in their outer shell which provides an element of spectral complexity compared to closed-shell molecules. Additionally, the most common isotope of lead, ^{208}Pb, has no nuclear spin, and there are two other even stable isotopes (^{204}Pb and ^{206}Pb) that provide useful tests of isotopic mass-scaling relationships. We will discuss this mass-scaling in more depth later in this chapter. Like ^{171}Yb, ^{207}Pb has a nuclear spin of $\frac{1}{2}-$, making it a useful bridge between analyzing the even isotopologues of PbF and the more complicated isotopologue ^{205}PbF, which requires the addition of an eQq term. PbF has the added simplification that its ground electronic state is a $^2\Pi_{1/2}$ state and its first excited electronic state is a $^2\Pi_{3/2}$ state, which means that most of the parameters used to describe these two states are the same, unlike the YbF case, which has $^2\Sigma^+$ orbital character in its ground electronic state and $^2\Pi_{1/2}$ orbital character in its first excited electronic state. While we mostly concern ourselves with the ground state of PbF in our analysis, the first excited state is relevant to the optical Fourier transform data that comprises a significant portion of the dataset.

This work is an extension of previous analyses of PbF presented by Ziebarth, *et. al.* [14], Alex Baum '11 in his senior thesis [5], Lukas Alphei (in German) [17], Alphei, *et. al* [8], and Mawhorter, *et. al* [13]. Thus, we adopt similar effective Hamiltonians to describe the molecule in this analysis. A fairly complete derivation of the matrix elements of these

Hamiltonians was provided by Alphei; here we will summarize the parameters of the model and their significance.

First note that we have a choice in how we couple angular momenta together in our model in order to arrive at the final energy states of the molecule. While these final states are physical, any intermediate states are model-dependent. However, choosing quantum numbers and the significance of their coupling wisely can often provide physical insights, so it is in our interests to find good quantum numbers to describe the system. Hund's cases are idealized cases which suggest good quantum numbers, so in practice we want to find the character of one or more Hund's cases in our molecule to simplify our analysis. While this simplification was computationally necessary in the past, modern computers can trivially analyze molecules in non-ideal Hund's cases. Alphei observes that PbF is generally described by Hund's case (a) for low rotational levels and moves to Hund's case (b) with higher rotational energy. This classification of Hund's cases is relevant to the parameter choice that follows. For a more complete overview of Hund's cases and their properties, see Glassman [21].

Before discussing the effective Hamiltonians and their parameters, we will briefly describe the quantum numbers used to describe transitions and their significance. The number $\boldsymbol{N}$ describes the end-over-end rotation of the molecule. This couples with the unpaired electron spin to form the quantum number $\boldsymbol{J} = \boldsymbol{N} + \boldsymbol{S}$. This coupling can be the cause of some confusion; generally $\boldsymbol{J}$ and $\boldsymbol{N}$ are equal to one another since most molecules do not have unpaired electron spins, and thus they are used interchangeably in some texts. However, here we are careful to distinguish between them. The quantum number P represents the parity of the state, and is given as $+1$ or -1 (or sometimes $+$ or $-$). These three quantum numbers, in conjunction with the vibrational level v, completely describe the even-isotope optical data used in our analysis. In most isotopologues of PbF, we only need the fluorine nuclear spin $\boldsymbol{I}_F$ to incorporate hyperfine splittings into the analysis via the quantum number $\boldsymbol{F} = \boldsymbol{J} + \boldsymbol{I}_F$. When Pb has nonzero nuclear spin, the intermediate number $\boldsymbol{F}_1 = \boldsymbol{J} + \boldsymbol{I}_{Pb}$ couples to $\boldsymbol{I}_F$ to yield $\boldsymbol{F} = \boldsymbol{F}_1 + \boldsymbol{I}_F$.

In the following discussion of the relevant parameters to our analysis of PbF, we use the n subscript to denote the electronic state of the molecule (restricted to the lowest two states, $^2\Pi_{1/2}$ and $^2\Pi_{3/2}$, in our analysis) and the v subscript to represent the vibrational energy level ($v = 0$ or $v = 1$ in our data). The general form of the effective Hamiltonian we use to analyze PbF is given by Mawhorter, *et al.* as

$$\boldsymbol{H}_{\text{eff}} = \boldsymbol{H}_{\text{spin-rotation}} + \boldsymbol{H}_0 + \boldsymbol{H}_1 + \boldsymbol{H}_{\text{ext}}, \tag{3.4}$$

where $\boldsymbol{H}_{\text{spin-rotation}}$ contains spin-rotation interactions of magnitude 5 - 50 GHz, $\boldsymbol{H}_0$ describes hyperfine structure of magnitude 0.2 - 10 GHz, $\boldsymbol{H}_1$ contains corrections to the hyperfine

structure arising from the interactions of three angular momenta of order 10 - 100 kHz, and $\boldsymbol{H}_{\text{ext}}$ describes the molecule's interactions with external fields [13]. This effective Hamiltonian neglects the absolute energy terms T_n and G_{nv}, which represent absolute energy offsets for the electronic and vibrational energy, respectively. Since we are interested in energy differences corresponding to transitions in our analysis, these terms are not included here.

The rotational Hamiltonian is determined chiefly by the fine-structure energy A, the rotational constant B, the fine-structure constant p. These terms also have higher-order corrections A_D, A_H, and p_D, which account for distortions due to the anharmonicity of the potential well of the system (see Figure 9). The rotational energy levels correspond to the eigenvalues of this Hamiltonian as given by Mawhorter, *et al.* in Equation (1) [13], but Alphei also gives an overview term by term which we will summarize here [17]. The rotational energy levels are defined by the Hamiltonian equation

$$\boldsymbol{H}_{\text{rotation}} = B_{nv}\boldsymbol{N}^2. \tag{3.5}$$

The spin orbit interaction given by

$$\boldsymbol{H}_{\text{givenbyspin}-\text{orbit}} = A_{nv}(\boldsymbol{L}\cdot\boldsymbol{S}) \tag{3.6}$$

represents the familiar interaction between the electron spin ($\boldsymbol{S}$) and the orbital angular momentum ($\boldsymbol{L}$) corresponding to its electronic state, which determines the splitting between electronic states. In PbF this splitting is quite large, so the states do not perturb one another significantly. Finally, the Λ-doubling parameters q_{nv} and p_{nv} arise from further coupling between $\boldsymbol{J}$ and $\boldsymbol{S}$, but Alphei notes that q_{nv} can be neglected in this instance. A further parameter than could appear here is the spin-rotation parameter γ, but it can generally be neglected in Hund's case (a) molecules where $A >> \gamma$. Since we do not explicitly fit γ, its character is absorbed in A, A_D, and A_H leading to the notation $\tilde{A}$, $\tilde{A_D}$, and $\tilde{A_H}$ in Alphei and Mawhorter, *et al.*

The hyperfine Hamiltonian involving the interaction of the electron and nuclear spins is characterized by the tensor $\hat{\boldsymbol{A}}$ (distinct from the spin-orbit parameter A). For PbF, it is

$$\boldsymbol{H}_0 = \boldsymbol{I}'_{Pb}\cdot\hat{\boldsymbol{A}}_{Pb}\cdot\boldsymbol{S}' + \boldsymbol{I}'_{F}\cdot\hat{\boldsymbol{A}}_{F}\cdot\boldsymbol{S}', \tag{3.7}$$

where primes represent the body-fixed frame of the molecule instead of the laboratory frame assumed in unprimed parameters. These interactions couple the nuclear spin $\boldsymbol{I}$ to the electron spin. Note that the only isotope of lead in our analysis with nonzero nuclear spin is ^{207}Pb, so parameters relating to the nuclear spin of lead will only appear in our analysis of ^{207}PbF (and in later predictive work of ^{205}PbF). The interactions in the hyperfine Hamiltonian can be further expanded to yield the parameters $A_{\parallel}$ and $A_{\perp}$, which have fixed relations to the

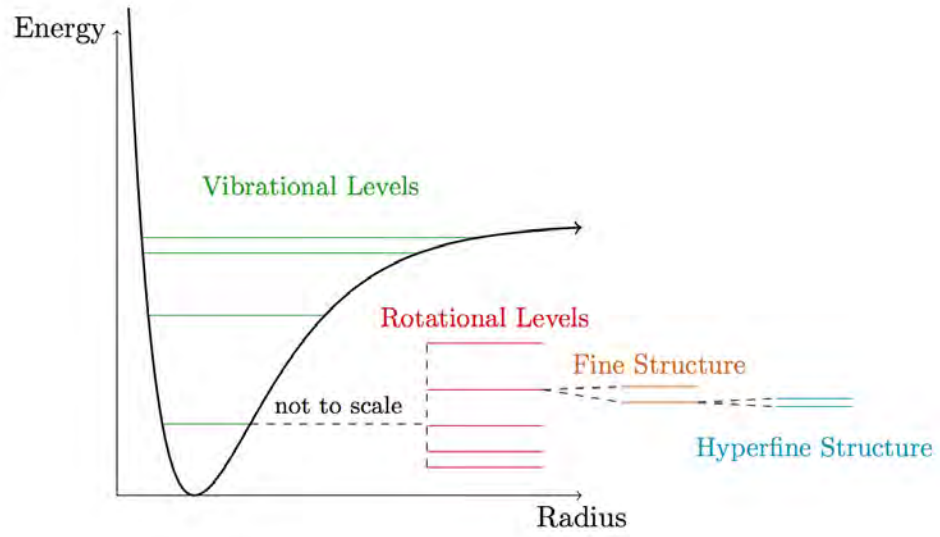

Figure 9: An example of a diatomic molecule's potential well. Within each vibrational level, there are splittings due to the rotational energies of the molecule, fine structure effects, and hyperfine effects, generally in order of decreasing magnitude. From [21].

Frosch & Foley parameters a, b, c, and d. See Mawhorter *et al.* for more details on these expansions and parameter relations [13].

The rest of the parameters in our analysis are contained in the Hamiltonian

$$\boldsymbol{H}_1 = (C_{Pb}\boldsymbol{I}_{Pb}\cdot\boldsymbol{J}+C_F\boldsymbol{I}_F\cdot\boldsymbol{J})-t_0[3(\boldsymbol{I}'_{Pb}\cdot\boldsymbol{n}')(\boldsymbol{I}'_F\cdot\boldsymbol{n}')-(\boldsymbol{I}_{Pb}\cdot\boldsymbol{I}_F)]+(d_{C_{Pb}}\boldsymbol{I}_{Pb}\cdot\boldsymbol{J}+d_{C_F}\boldsymbol{I}_F\cdot\boldsymbol{J})(\boldsymbol{J}'\cdot\boldsymbol{S}'), \tag{3.8}$$

where $\boldsymbol{n}'$ gives the direction of the internuclear axis. The C_{Pb}, C_F, and t_0 parameters govern the interaction of the nuclear magnetic moments with the rotation of the molecule and themselves, while Petrov, *et al.* have shown that the $d_{C_{Pb}}$ and d_{C_F} parameters give a centrifugal correction to the hyperfine $A_\perp$ parameters [48].

For a visual representation of the magnitudes of the various effects described by the effective Hamiltonian parameters and interactions, see Figure 10. Finally, note that our analysis focuses on PbF in the absence of external electric and magnetic fields, so the contributions of $\boldsymbol{H}_{\text{ext}}$ are assumed to be zero. Explorations of Zeeman splitting and other external field effects have been previously performed [13], [5], [49].

3.2.2 Dunham Formulation

In order to fit a multitude of data sets across isotopologues of PbF, we adopted a Dunhuam-style expansion of the paramters with assumed isotopic mass scaling. The Dunham formulation provides a more flexible potential well than the traditional Morse potential by expanding each parameter in a power series of vibrational corrections. These expansions can

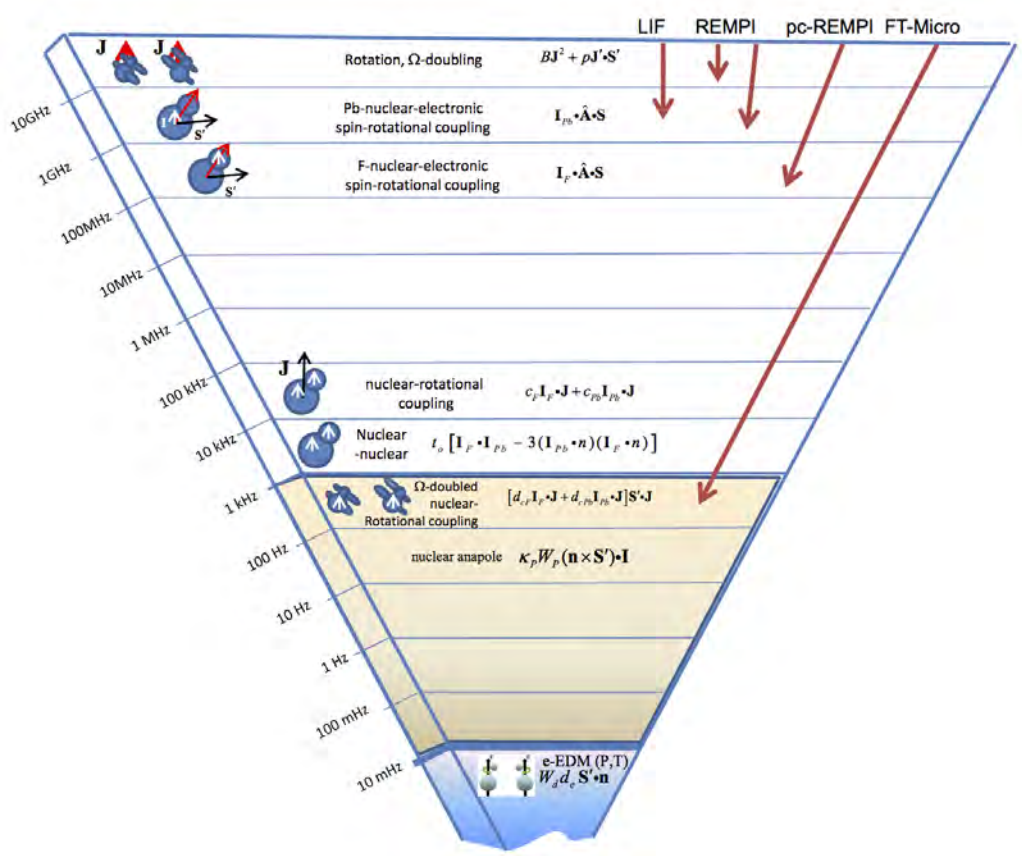

Figure 10: The frequency scale of various effects in PbF and the resolution of various spectroscopic methods, including the Fourier-transform microwave method used in this thesis that presents a roughly five order of magnitude improvement in sensitivity versus other methods. Note that some parameters are defined with slightly different quantum numbers than in the text; since most molecules do not contain unpaired electrons, it is often assumed that $\boldsymbol{J} = \boldsymbol{N}$ and the two are used interchangeably; however, in the case of PbF, the two differ by the addition of the unpaired electron spin $\boldsymbol{S}$. Adapted from [50].

be performed both on the rovibrational parameters, where they are explicitly defined as

$$B_v = \sum_{l=0} Y_{l,1} \left(v + \frac{1}{2}\right)^l, \tag{3.9}$$

$$D_v = \sum_{l=0} Y_{l,2} \left(v + \frac{1}{2}\right)^l, \tag{3.10}$$

$$H_v = \sum_{l=0} Y_{l,3} \left(v + \frac{1}{2}\right)^l, \tag{3.11}$$

(the $Y_{l,m}$ are distinct from the spherical harmonic functions) and other parameters, via the relations

$$X_v = \sum_{l=0} X_{l,0} \left(v + \frac{1}{2}\right)^l, \tag{3.12}$$

$$X_{D_v} = \sum_{l=0} X_{l,1} \left(v + \frac{1}{2}\right)^l, \tag{3.13}$$

$$X_{H_v} = \sum_{l=0} X_{l,2} \left(v + \frac{1}{2}\right)^l. \tag{3.14}$$

Our analysis does not include any second-order rotational corrections in the form of H_v or X_{H_v}, but they are included above for completeness.

In addition to this vibrational expansion, the Dunham fitting procedure assumes a reduced mass scaling relation between the isotopologues of the molecule. This scaling is given by the relations

$$Y_{l,m} = U_{l,m} \left(\frac{1}{\mu}\right)^{\frac{l}{2}+m} \left(1 + \frac{\Delta^F_{l,m} m_e}{M_F} + \frac{\Delta^{Pb}_{l,m} m_e}{M_{Pb}}\right) \tag{3.15}$$

$$X_{l,m} = U^X_{l,m} \left(\frac{1}{\mu}\right)^{\frac{l}{2}+m} \left(1 + \frac{\Delta^{X,F}_{l,m} m_e}{M_F} + \frac{\Delta^{X,Pb}_{l,m} m_e}{M_{Pb}}\right) \tag{3.16}$$

where $X = \mathrm{A}$, $A_\perp$, $A_\parallel$, t_0, $p_{C_{Pb}}$, and p_{C_F},

$$X'_{l,m} = U^{X'}_{l,m} \left(\frac{1}{\mu}\right)^{1+\frac{l}{2}+m} \left(1 + \frac{\Delta^{X',F}_{l,m} m_e}{M_F} + \frac{\Delta^{X',Pb}_{l,m} m_e}{M_{Pb}}\right) \tag{3.17}$$

where $X' = C_{Pb}$. C_F, and p.

$U_{l,m}$ is the mass-independent Dunham parameter that is scaled by the reduced mass ratio of the isotopologue to a reference isotopolouge (^{208}PbF in our case), and $\Delta^{X,Pb}_{l,m}$ is the isotope-independent Born-Oppenheimer breakdown (BOB) term [51]. The BOB term allows the model to deviate from the strictly assumed reduced mass scaling, and represents a breakdown in the model's assumption that the nucleus is infinitesimally small. Since lead is a relatively heavy nucleus, we expect rather large BOB terms for PbF, as have been seen in other lead compounds such as PbSe and PbTe [52]. We do not isotopically vary the Fluorine in our analysis, so the corresponding BOB term can be neglected.

Finally note that hyperfine parameters require magnetic moment scaling as well. The ratio of this scaling is proportional to the magnetic moment ratio and inversely proportional to the nuclear spin of the isotope. However, this scaling is only necessary when both isotopes have a nuclear magnetic moment, g_N. In lead, the only stable isotope with nonzero g_N is ^{207}PbF, so we do not implement this kind of scaling in the global fit. However, to predict the spectrum of ^{205}PbF, this scaling does become important.

3.2.3 Potential Applications of PbF

The most enticing feature of the PbF molecule is the low-lying nearly degenerate states of opposite parity in ^{207}PbF. Applications of this molecule all focus on ways to take advantage of these states, which can be seen in Figure 3 in Section 1.2. While the $v = 1$ state of ^{207}PbF or ^{205}PbF could exhibit even closer degeneracy in these states of opposite parity, the amount of degeneracy observed in ^{207}PbF could already prove applicable to cutting edge experiments in physics, such as a measurement of the eEDM, the parity violating nuclear anapole moment, or variation in the fundamental constants.

As has been previously discussed in Chapters 1 and 2, this accidental degeneracy is instrumental in suppressing systematic errors in an eEDM measurement. Since the states are of opposite parity levels, their proximity amounts to spectroscopically reversing the effective electric field experienced by electrons transitioning to these states. In previous eEDM experiments, such as the YbF result, the electric field polarity was manually reversed in the laboratory. While this method also reverses the effective electric field affecting the electrons in the experiment, it is much more prone to leakage currents and other stray effects resulting from switching the field macroscopically. Thus ^{207}PbF's energy structure is highly favorable for an eEDM measurement with fewer systematic errors.

PbF's other advantageous feature for eEDM experiments is its relatively small magnetic g-factor in its ground state. This feature means the molecule is not very sensitive to external magnetic fields, providing protection against another common systematic error in the form of stray magnetic fields. The g-factor is a state-dependent value, characterized given by the equation

$$g_J = \frac{(\Lambda + g_s\Sigma)|\Lambda + \Sigma|}{J(J+1)}, \tag{3.18}$$

where $g_S = 2.00232$ is the electron g-factor and for a $^2\Pi_{1/2}$ state $\Lambda = \pm 1$ and $\Sigma = \mp\frac{1}{2}$, leading to a near cancellation of the molecular g-factor in PbF's ground state. It can be further characterized through the state-independent body-fixed G-factors, $G_\parallel$ and $G_\perp$. The body-fixed G-factors of ^{208}PbF have also been the subject of theoretical and experimental study [5], [49]. This work links to the determination of an eEDM measurement in several ways. Most immediately, refined g-factor values allow for better estimates of systematic errors in an eEDM measurement. More indirectly, *ab initio* calculations of the body fixed G-factors and their comparison with experimental values can serve as a method of checking the theoretical understanding of the PbF system and, by extension, other molecular systems used for eEDM experiments. Since the effective electric field at the nucleus is a theoretically derived value, this step can serve as another way of validating a final value for an eEDM measurement.

Motivated in part by existing proposals for experiments in the PbF system, Flambaum,

et al. proposed a study of variation in the fundamental constants in ^{207}PbF [53]. Such experiments would also take advantage of the closely spaced energy levels of opposite parity in the ground state of ^{207}PbF, in this case for precision measurement of the transition frequency between the two levels, ω. The paper derives the numerical sensitivity to variation in various fundamental constants of interest, summarized in the equation

$$\frac{\delta\omega}{\omega} \approx -55\frac{\delta\alpha}{\alpha} + 2.1\frac{\delta(m_q/\Lambda_{\mathrm{QCD}})}{(m_q/\Lambda_{\mathrm{QCD}})} + \frac{\delta(m_e/m_p)}{(m_e/m_p)}, \tag{3.19}$$

where α is the fine structure constant, m_q/Λ_{QCD} is the the quark mass over the QCD scale, and m_e/m_p is the ratio of the electron mass and the proton mass, and the sensitivity constants carry an uncertainty of around 20%. Due to the large enhancement factor of the fine structure constant portion of this equation, PbF is suited towards placing more sensitive limits on variation in the fine structure constant $\dot{\alpha}$, in addition to the other promising fundamental physics experiments discussed earlier.

4 Spectroscopic Measurements of PbF

The goal of any spectroscopic analysis is to determine the internal energy levels of some system—in the case of this thesis, the diatomic molecule lead fluoride. These levels are generally ordered according to splittings of various magnitudes in energy, which the spectroscopic model seeks to account for in terms of theoretically motivated effects. See Figure 9 for a visualization of the splittings in a generic diatomic molecule. Since different spectroscopic experiments can probe these levels with varying degrees of energy resolution, not all of these splittings are resolved in every experiment.

Conceptually, spectroscopic measurements follow a fairly basic experimental approach. In order to determine the internal energy level structure of a sample, such as a particular kind of molecule, transitions between energy levels in the sample must be observed. Assuming the sample is initially in its ground state, it can be excited via a source of electromagnetic modes that encompasses some range of energies (which are easily converted to frequencies via a factor of Planck's constant for a complementary way to think about the experiment). At this stage, there are two ways to proceed in measuring any potential transitions; it is possible to wait for the sample to decay to collect the frequency of radiated light, or alternatively, one could collect the light that was not absorbed by the sample in the excitation step. Which of these methods to pursue depends on experimental details, but both provide the same physical information. By carefully assigning the transitions to internal states represented by unique quantum numbers, it is usually possible to experimentally determine the spectroscopic model of the system in question. Assigning quantum numbers can be difficult or even intractable at arbitrary levels of precision without a previous understanding of the system at hand, making spectroscopy an iterative process. Lower resolution data can provide the firm foundation on which to build more precise measurements and models.

4.1 Experimental Details

In this analysis, we use data from two different experiments that span the stable isotopologues ^{204}PbF, ^{206}PbF, ^{207}PbF, and ^{208}PbF, the vibrational levels $v = 0$ and $v = 1$, and the ground and first excited electronic states ($^2\Pi_{1/2}$ and $^2\Pi_{3/2}$, respectively). The focus of our analysis is on the ground electronic state, and the large spacing between the first electronic state and the ground electronic state allows us to neglect perturbative interactions between the two (unlike for example BrO [54]).

A large portion of the data in this thesis was provided by E. H. Fink and his group. Some of this data has previously analyzed and published [14], and there is also a detailed description of the experiment in the literature [55]. The data provided by Fink *et al.* are comprised of Fourier-transform infrared measurements which resolve fine structure in the PbF spectra.

This frequency region encompasses transitions from the first excited electronic state to the ground state, enabling the characterization of both electronic states. Additionally, this data includes a high range of rotational energies since it was conducted at room temperature. Previously analyzed data included in our global fit is comprised of 231 ^{208}PbF, 212 ^{207}PbF, and 195 ^{206}PbF $v = 0 \rightarrow v = 0$ transitions ranging from rotational number $J = 0.5$ to $J = 54.5$. Additionally, Fink provided raw data for bands corresponding to ^{208}PbF and ^{207}PbF $v = 1 \rightarrow v = 1$ transitions, from which we assigned a further 22 ^{208}PbF and 27 ^{207}PbF transitions.

To complement this infrared data, our analysis includes high resolution Fourier-transform microwave data that directly probes hyperfine transitions in a rotationally cooled ($J = 0.5$ to $J = 3.5$), ground state sample of PbF in both the $v = 0$ and $v = 1$ vibrational states. Currently included in the fit are 19 ^{208}PbF, 31 ^{207}PbF, and 12 ^{206}PbF $v = 0$ transitions and 6 ^{208}PbF, 4 ^{207}PbF, and 6 ^{206}PbF $v = 1$ transitions. Some of this data was previously taken and analyzed by isotopologue [8], [13]. The several orders of magnitude improvement in precision over the IR data not only provides better resolution of some fine structure constants, but also yields information about hyperfine constants that are not resolved at lower resolution. However, this data does not provide much or any information about the first excited electronic state or rotational anharmonicity in the potential, so combining these two sources of data into one global fit provides a much more complete picture than the individual analyses that currently exist.

4.1.1 Fourier Transform Microwave Setup

Fourier-transform microwave (FTMW) data was taken with an apparatus located at the Leibniz Universität in Hannover, Germany. While we give an experimental overview here, more detail can be found in published descriptions of the device [56], [57]. This spectrometer consists of a large vacuum chamber with two spherical aluminum mirrors forming a Fabry-Perot cavity (see Figure 11). This cavity, in conjunction with a microstepper motor to control one of the mirrors allows the spectrometer to be highly sensitive to resonances in the sample with full-width half-maximum of around 10 KHz and to accuracies better than 1 KHz. The total range of frequencies of this arrangement is from around 2 to 26.5 GHz with mode widths of 0.25 - 1 MHz from low to high frequency.

To obtain the desired PbF sample, a lead rod is ablated with a high power Nd:YAG laser in the presence of a mixture of 99% neon gas and 1% SF_6. Some of the vaporized lead bonds with fluorine donated by the SF_6 to form PbF in the vapor. While other chemical compounds and free atoms exist in the vapor, the selectivity of precision provided by the cavity means that other transitions rarely, if ever, appear in the signal. A much larger problem due to this level of precision is that it can be difficult to find transitions without good predictions

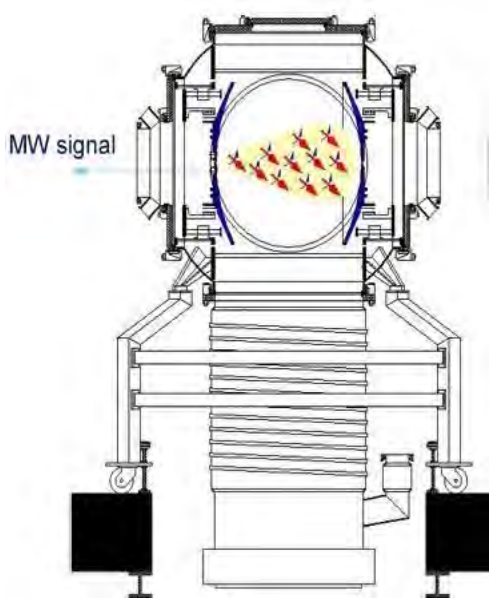

Figure 11: A schematic of the microwave spectrometer used to collect Fourier-transform microwave data used in our analysis. A cryogenic beam of sample molecules in buffer gas is injected into the resonant cavity coaxially with the mirrors and excited with a microwave burst. The subsequent decay is precisely monitored by adjusting the spacing of the mirrors in the cavity.

beforehand given the narrow mode widths discussed above.

The vapor containing the molecule of interest, in this case PbF, then expands into the vacuum chamber. The supersonic expansion that the gas undergoes at this stage cools the molecules to exist primarily in the ground state at a rotational temperature of a few Kelvins. A consequence of this cooling is that the signal of excited vibrational levels and higher rotational levels are significantly weaker than their corresponding ground states, at about 15 orders of magnitude per vibrational level. The sample is injected coaxially with the mirrors through a small hole in one of the mirrors, a design that provides better sample-mode overlap in the resonant cavity as it travels between the mirrors, yielding more sensitivity relative to the traditional perpendicular arrangement (see, for example, uncertainties provided in Lesarri, *et. al* [58]).

As the vapor expands into the cavity, sample molecules are coherently excited via a short microwave burst. Once the burst ends, the excited polarized molecules undergo free induction decay back to their ground state. The resulting microwave emission is collected by a set of small antennas located near the center of one of the mirrors, with signal intensity strongly dependent on the resonance associated with transitions between energy levels.

From this brief description of the apparatus, it is clear that there are many tunable parameters in the experiment, including the laser power, the amount of gas to inject with each shot, and the ablation laser-gas valve timing. In practice, these parameters are all

manipulated while observing a well-known strong transition to optimize the intensity. An additional change that can be made is swapping the noble buffer gas from neon to argon. Typically, the buffer gas is chosen to match the mass of the desired molecular sample for optimal cooling, but for PbF we found that neon yielded better results.

A further tunable parameter relevant to the open shell molecule PbF is the magnetic field in the cavity. Since the focus of this study excluded Zeeman splitting effects, it is desirable that zero magnetic field be seen by the molecules in the cavity. The Hannover FTMW apparatus is equipped with Hemholtz coils in three axes around the cavity, which can be tuned to precisely cancel the magnetic field of the earth, as well as any other latent fields in the local environment. In practice, this field nulling is achieved by monitoring the Zeeman splitting in a few well-known transitions with high intensity and iteratively adjusting the current in each of the coils until no significant splitting is observed. For more details on the motivations on selecting which transitions to tune on, see Alex Baum '11's thesis [5].

4.1.2 Analysis of Raw Microwave Data

Since the motion of the vapor as it expands into the cavity is mainly parallel to the mirrors, the microwave signal produced by the decay of the molecules from their excited state naturally exhibits Doppler shifts corresponding to emission parallel or antiparallel to the molecular motion. This Doppler shift is an experimentally advantageous feature; any "real" signal will necessarily appear as a pair of lines, reducing the probability of misidentification of noise peaks as a transition. The true transition frequency lies within negligible distance of the arithmetic mean of the two Doppler shifted peaks, which is assigned as the measured transition frequency. The magnitude of Doppler splitting is frequency and buffer gas dependent, but can be determined on a given day using a well-known transition. Once the shift is known at a particular frequency, it can be used to judge whether a particular transition at a different frequency exhibits the expected amount of Doppler splitting. See Figure 12 for a typical measurement of a transition and its corresponding Doppler peaks in the ftmw++ program that interfaces the computer with the FTMW apparatus.

Once a transition has been observed, it still remains to assign the correct set of quantum numbers to that transition. This step is where an existing model is integral to the operation of the FTMW spectrometer; generally the transition in question is already approximately known along with its quantum numbers. In our case, lines are predicted and then fit to a model using the SPCAT/SPFIT suite programmed by Herb Pickett. Operation of SPFIT and SPCAT has been described in the official manual [59] as well as other student theses [21], [60].

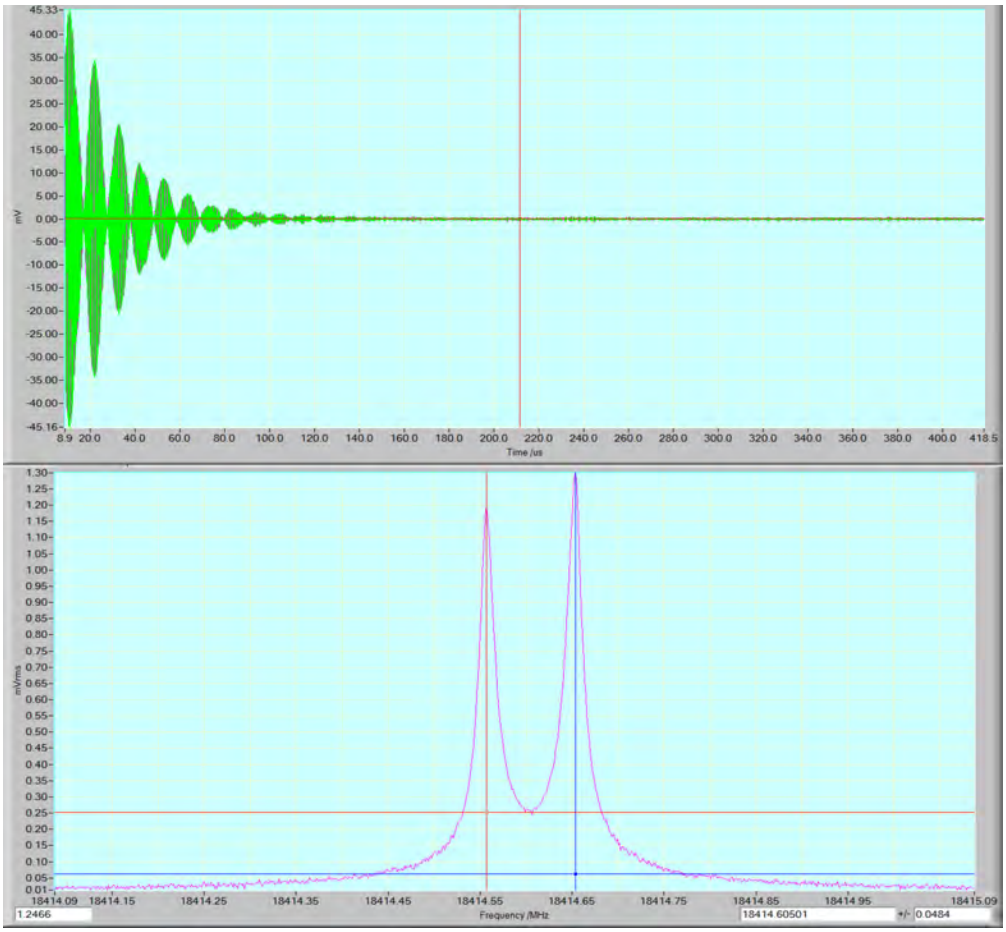

Figure 12: The upper image is a screen shot of the time domain of a typical FTMW signal in ftmw++. The Fourier-transformed signal is on the bottom, which also shows a center frequency and doppler shift offsets from the center in the bottom right corner.

4.2 Fitting Routine

Closely linked to the predictive program SPCAT is the fitting program SPFIT. Given a set of transition frequencies with associated quantum numbers and a starting set of parameters that are reasonably close to their "true" value, SPFIT runs an iterative algorithm on the floating parameters to minimize the root mean squared (RMS) error of the fit. The RMS is defined as

$$\sigma = \sum_{i=1}^{N} \sqrt{\frac{(o_i - c_i)^2 w_i}{\delta_i^2 n}}, \tag{4.1}$$

where N is the number of lines, δ_i is the measurement uncertainty, o_i is the observed transition frequency, c_i is the calculated transition frequency, and w_i is a weight determined by the smallest uncertainty squared divided by the measurement uncertainty squared. Therefore, our fit weights the most certain lines much more heavily than lines that are not as well de-

termined. It is expected that a fit will have an RMS of 1 if the errors are correctly assigned, since this indicates that around 68% of lines fall within 1-σ error bars of the calculated values, which is the expected result. In practice, a large global fit is still assumed to be correct with an RMS 10-30% higher than 1. An RMS lower than 1 generally indicates the error bars have been overestimated.

As described by Glassman, SPFIT can be used to perform a global Dunham fit [21]. Here this kind of fit is enabled by scaling parameters for each isotopologue and vibronic state and fixing their expected ratios. To ensure this rather complicated process is error-free and weight each set of data approriately, it is useful to fit individual data sources and isotopologues on their own and then incrementally combine them. Indeed, we fit each isotopologue's microwave and IR data individually, combined them by isotopologue, and produced global fits of each kind of data before attempting to combine all of the data into one global fit.

4.3 Results

After implementing a fit of each isotopologue on its own, first by data type and then across data types, a global fit of all data for all isotopologues (83 FTMW transitions, including 16 new in this work, and 608 FTIR transitions) was implemented using the Dunham style vibrational expansions and isotopic mass scaling schemes described above. Since the only isotope of lead with nonzero magnetic moment in the fit is ^{207}PbF, no magnetic moment scaling was implemented in this global fit. One additional subtlety beyond the theory presented earlier arises in the slight dependence of the A_{00} parameter on the Pb isotope in question, as seen in Table I of Mawhorter, *et al.* Although the parameter depends on the equilibrium bond length of the potential, it scales with isotopic mass due to differences in the zero point bond lengths. Here different values for each isotope both in our fits and in previous fits of A_0 [13] and an empirical scaling was employed for this parameter for each isotope according to the ratio of its values for ^{207}PbF and ^{208}PbF, using the available optical data of multiple vibrational levels for these isotopologues.

The current best fit parameters of the global fitting procedure can be found in Table 3. This model fits the data with an RMS of 4.54, which means it is not as precise as the uncertainties associated with our data. There are several clear indicators of systematic errors within the current global fit, which appear to center around an unknown inconsistency in the mass scaling applied to the parameters. Most of the optical transitions have a difference of larger than 0.002 cm^{-1} between the calculated and observed values; these differences appear systematic based on the isotopologue since the ^{208}PbF transitions are almost universally higher in frequency than predicted and the ^{206}PbF transitions are lower. Since it is the lower resolution optical data exhibiting this systematic error, it seems that the mass scaling in one

of the fine structure parameters—that is one of the Y, A, or p parameters, is incorrectly scaled with mass. This conclusion is supported by a global fit of all of the low resolution optical data alone, which has an RMS of 2.32 with current mass scaling assumptions. In light of the lack of formal theoretical motivation for the empirical isotopic scaling of A_{00}, it is clear that further understanding of mass scaling in fine structure parameters is required to resolve this problem.

Another issue apparent from comparing the predicted and observed values for the optical transitions is the poor fit of the $v = 1 \rightarrow v = 1$ transitions for ^{208}PbF and especially ^{207}PbF. While it is possible that the fits are affected by the overwhelming volume of $v = 0$ optical transitions, biasing the model towards fitting that regime well, it is also possible that the quantum number assignments for these transitions should be revised. This assignment is especially difficult for the extremely dense ^{207}PbF IR spectrum, making it another possible contributor to the enlarged RMS of the global fit.

The microwave data exhibits less obvious systematic errors, but the current model does not predict these transitions as accurately as their uncertainties are reported either. It is likely that the mass scaling affecting the lower resolution data is similarly affecting the fit of the hyperfine transitions. While the hyperfine parameters may be able to compensate for this incorrect scaling in part, these parameters are small enough that even little changes to rotational or spin-orbit parameters could change their behavior. Thus, the findings regarding small hyperfine parameters and BOB terms presented here should be taken with a grain of salt; they will be much better supported once the RMS of the global fit is closer to 1.

4.3.1 Born-Oppenheimer Breakdown Findings

From table 3, we can see that two Born-Oppenheimer breakdown terms were resolved. The most common BOB term, corresponding the lowest-order rovibrational parameter, is given in the fit by the relation

$$U_{01}\Delta_{01}^{Pb} m_e/(\mu M_{Pb}) = -0.3879(44). \tag{4.2}$$

Isolating the mass independent BOB term yields

$$\Delta_{01}^{Pb} = -21.2(2), \tag{4.3}$$

which is consistent with the sign found in PbTe (-11.56(15)) and PbSe (-12.92(24)) [52] but agrees in magnitude with the value reported for PbI (18.5(60)) [61]. A similar analysis for the BOB term corresponding to the p_{00} parameter yields

$$\Delta_{00}^{p,Pb} = 108.2(11), \tag{4.4}$$

which seems large, although no direct comparison is available. These results are preliminary in light of the known mass scaling errors present in the current global fit. It seems likely that BOB terms are particularly sensitive to systematic errors in mass scaling, since they correct for such errors at high levels of precision.

Table 3: PbF Parameters Derived From Global Fit [a]

Parameter	Isotopic Scaling	Value in MHz (Unc.)
U_{01}/μ	μ^{-1}	6937.7387(73)
$U_{01}\Delta_{01}^{Pb}m_e/(\mu M_{Pb})$	$(\mu M_{Pb})^{-1}$	-0.3879(44)
Y_{11}	$\mu^{-3/2}$	-44.3877(626)
$Y_{02}\times 10^3$	μ^{-2}	-5.1690(172)
A_{00}	1	247725910.5(93)[b]
A_{10}	$\mu^{-1/2}$	781328(126)
A_{01}	μ^{-1}	157.6182(117)
A_{11}	$\mu^{-3/2}$	0.1338(126)
$A_{02}\times 10^3$	μ^{-2}	0.15608(290)
U_{00}^{p}	μ^{-1}	4141.4606(122)
$U_{01}^{p}\Delta_{00}^{p,Pb}m_e/(\mu M_{Pb})$	$(\mu M_{Pb})^{-1}$	1.182(12)
p_{10}	$\mu^{-3/2}$	1.812272(316)
$p_{01}\times 10^3$	μ^{-2}	3.1888(100)
$A_{\perp_F 00}$	g_N	255.05065(492)
$A_{\perp_F 10}$	$g_N\mu^{-1/2}$	1.87592(612)
$A_{\parallel_F 00}$	g_N	-411.34737(115)
$A_{\parallel_F 10}$	$g_N\mu^{-1/2}$	2.9918(136)
c_{F00}	$g_N\mu^{-1}$	0.021113(153)
$c_{F10}\times 10^3$	$g_N\mu^{-3/2}$	-0.472(200)
$d_{c_F 00}\times 10^3$	$g_N\mu^{-1}$	1.077(418)
$A_{\perp_{Pb} 00}$	g_N	$-7247.0462(542)$[c]
$A_{\perp_{Pb} 10}$	$g_N\mu^{-1/2}$	$-33.9487(107)$[c]
$A_{\parallel_{Pb} 00}$	g_N	$-10132.0988(54)$[c]
$A_{\parallel_{Pb} 10}$	$g_N\mu^{-1/2}$	$-27.2166(106)$[c]
c_{Pb00}	$g_N\mu^{-1}$	$0.321365(129)$[c]
$d_{c_{Pb}00}\times 10^3$	$g_N\mu^{-1}$	$-9.26(80)$[c]
$t_{0\ 00}$	g_N	$-0.01589(54)$[c]

[a] The parameter values given here are for ^{208}PbF. Parameters for other isotopologues are derived from the isotopic scaling relations and magnetic moment ratios for isotopes of lead with nonzero magnetic moments given in the text, unless otherwise noted. While no magnetic moment (g_N) scaling was necessary for the global fit, it was implemented in predicting ^{205}PbF parameters.

[b] Individual fits of isotopologues exhibited slight A_{00} value differences. These differences were empirically implemented using the ratio of change of the parameter in the fits of ^{207}PbF and ^{208}PbF. This variation is due to the variation of the zero point bond lengths arising from mass differences in the isotopologues, while the theoretically expected lack of mass dependence of the parameter is because it depends on the equilibrium bond distance for the potential.

[c] This parameter applies only to isotopes of lead with nonzero nuclear spin. Value given as ^{207}PbF value.

5 Predictive Work

As previously discussed, one application of the robust global fit produced here is to use it for predicting the energy structure of PbF states with limited or unavailable data. Particularly, we will investigate the first excited vibrational level of ^{207}PbF and the ground vibrational level of ^{205}PbF for the presence of energy levels of opposite parity with closer near degeneracy than those found in the ground vibrational level of ^{207}PbF.

At the current level of accuracy in the global fit model, the 1σ observed minus calculated values are about 5 the expected uncertainty in a Fourier-transform microwave measurement of about 0.5 kHz. Hence with a more conservatice $w\sigma$ estimate we can still expect the current fit to be accurate to about 5 kHz in predicting these microwave transitions. The frequency separation of the two low lying states of opposite parity in ^{207}PbF is about 266 MHz (.00888 cm^{-}1), so an analysis accurate even to 10 kHz can still provide a useful platform for the first estimate of the presence of other nearly degenerate energy levels of opposite parity in various states of PbF.

5.1 Predicting Routine

Predictions were performed using the SPCAT program, which is the predictive analogue the analysis suite SPFIT. SPCAT takes in the relevant spins of a molecule, a parameter set (in the *.par* file), and a temperature, partition function, and dipole moment (in the $*.int$ file), and returns both a list of transition quantum numbers and their expected intensities at that temperature (called the $*.cat$ file) and a list of energy levels, their absolute energy, and their quantum numbers (called the $*.egy$ file). Since we only care about relative spacings of the states, we take the lowest absolute energy returned in the $*.egy$ file and subtract that value off of each of the absolute energies reported. Then the lowest energy level is the zero point and the rest of the energy levels reference up from it. SPFIT/SPCAT documentation exists in one file, and the shared structure of the programs means it is relatively easy to turn a fit from a $*.par$ file into a predictive $*.var$ file.

5.2 The ^{207}PbF $v = 1$ State

The existence of low lying energy states of opposite parity in the $v = 0$ state of ^{207}PbF has already encouraged predictions of experiments sensitive to fundamental physics. However, it is also worth investigating whether there is a perturbation to this system that will produce an even more attractive configuration for fundamental physics research. A rather obvious approach is to increase the vibrational energy level of the system, to see if this excitation pushes the already nearly degenerate states of interest closer together or drives them apart.

With our vibrationally sensitive dataset, we can investigate the $v = 1$ level of the system to see if these or any other states of opposite parity exhibit more near-degeneracy than has already been observed.

5.2.1 Results

The first 22 predicted energy levels for ^{207}PbF from the global fit for both the $v = 0$ and $v = 1$ states can found listed in Table 4, with the lowest 14 levels plotted in Figure 13 and the states of interest plotted in Figure 14. When comparing the $v = 0$ levels to those derived from a previous model, we see the expected agreement to within a few kilohertz, suggesting the $v = 1$ energies are also suitable preliminary predictions.

The levels of interest are levels 3 and 4, and the spacing between them in the $v = 0$ state is 266.28 MHz. The spacing between these levels in the $v = 1$ state is 233.54 MHz, which represents a roughly 12% closer spacing than in the $v = 0$ state. This preliminary result from our global fit strongly suggests suggests that $v = 1$ ^{207}PbF is a significantly better candidate than the ground vibrational level of ^{207}PbF for fundamental physics experiments.

Observing the 22 energy levels shown in Table 4 and more predicted levels not shown, it appears that the spacing between the analogous energy levels of opposite parity increases as J increases. From our vibrational analysis, the shifts in energy levels caused by vibrational excitation appear to be much smaller than the spacings at higher J than the $J = \frac{1}{2}$ levels 3 and 4. Thus, states 3 and 4 represent the most degenerate low-lying states of opposite parity that have been observed in ^{207}PbF.

A natural next question suggested by these results is whether the spacing of states 3 and 4 is further reduced by higher vibrational excitations. In order for the global fit to accurately predict the structure of $v = 2$ energy levels and beyond, some vibrational data from these states would be required. Thus, the current model cannot directly inform the structure of $v = 2$ and higher vibrational energies of PbF, but it does provide an excellent foundation for such an analysis once more vibrational data is obtained. As the FTMW signals for $v = 1$ transitions were about a factor of 15 weaker than for $v = 0$, and a similar decrease is to be expected from $v = 1$ to $v = 2$, this data collection is not a simple exercise under current experimental conditions.

Table 4: First 22 Predicted Energy Levels of ^{207}PbF

					Absolute Energy (MHz)		
Level	J	P	F_1	F	$v = 0$ (Previous) [13]	$v = 0$	$v = 1$
22	2.5	+	2	2.5	70 919.300	70 919.323	70 599.984
21	2.5	+	2	1.5	70 755.337	70 755.337	70 435.338
20	2.5	+	3	3.5	67 474.609	67 474.618	67 130.636
19	2.5	+	3	2.5	67 320.236	67 320.225	66 975.673
18	2.5	−	3	2.5	58 699.689	58 699.693	58 374.748
17	2.5	−	3	3.5	58 604.206	58 604.209	58 278.094
16	2.5	−	2	1.5	54 890.149	54 890.140	54 558.689
15	2.5	−	2	2.5	54 810.573	54 810.575	54 478.105
14	1.5	−	1	1.5	34 559.389	34 559.385	34 461.682
13	1.5	−	1	0.5	34 374.270	34 374.263	34 275.991
12	1.5	−	2	2.5	31 229.123	31 229.110	31 103.557
11	1.5	−	2	1.5	31 065.045	31 065.034	30 939.091
10	1.5	+	2	1.5	22 609.045	26 609.578	26 507.948
9	1.5	+	2	2.5	22 529.893	26 529.893	26 426.945
8	1.5	+	1	0.5	22 691.749	22 691.740	22 590.560
7	1.5	+	1	1.5	22 658.901	22 658.883	22 556.894
6	0.5	+	0	0.5	11 416.205	11 416.186	11 451.862
5	0.5	+	1	1.5	8 687.210	8 687.205	8 686.876
4	0.5	+	1	0.5	8 495.002	8 494.979	8 495.068
3	0.5	−	1	0.5	8 228.717	8 228.703	8 261.530
2	0.5	−	1	1.5	8 196.392	8 196.385	8 227.504
1	0.5	−	0	0.5	0	0	0

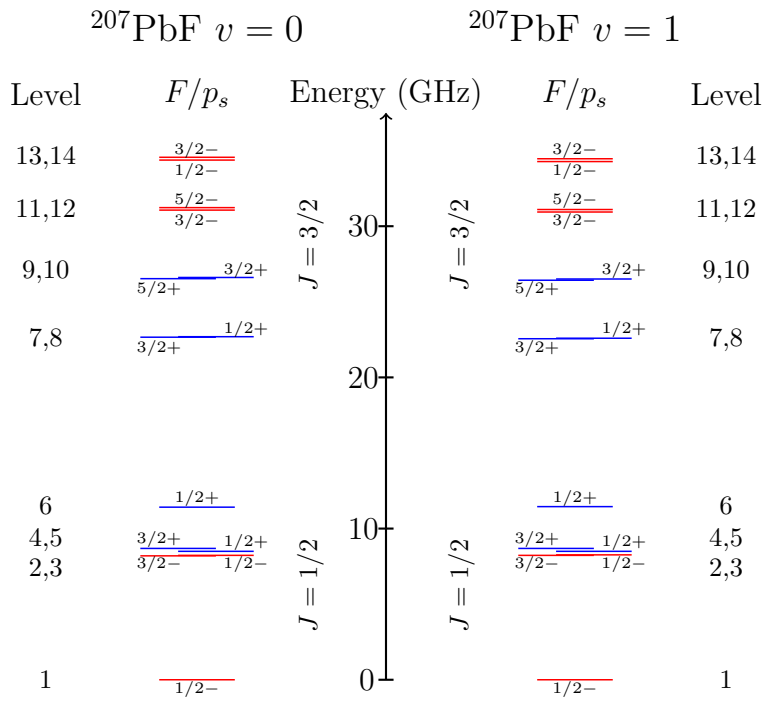

Figure 13: Predicted energy level diagrams of the low-lying states of ^{207}PbF with $v = 0$ levels on the left and $v = 1$ levels on the right. Parity has been labeled red/blue for $-/+$ parity, respectively.

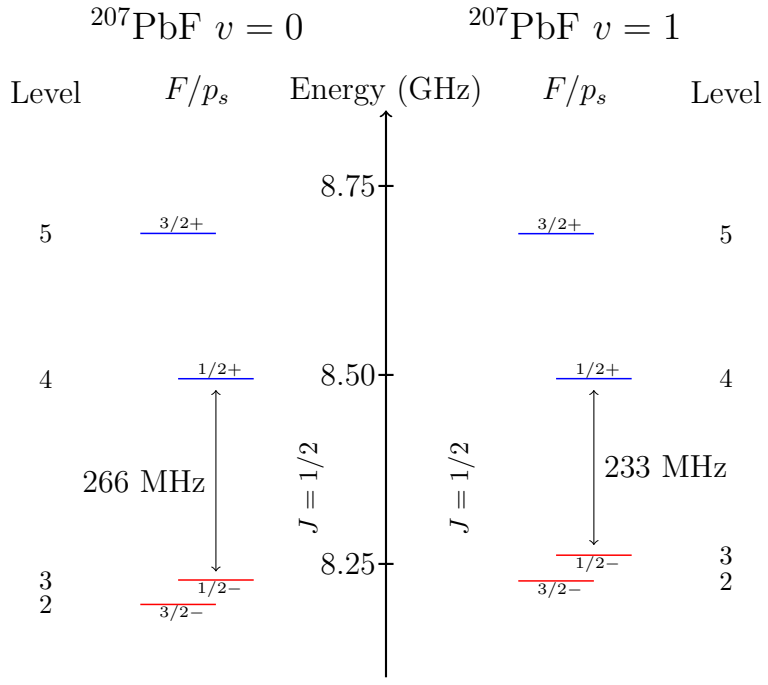

Figure 14: Energy level diagram of low-lying states of opposite parity in ^{207}PbF, with $v = 0$ on the left and $v = 1$ on the right. The spacing between states of interest in the $v = 1$ state is about 12% closer than the equivalent spacing in the $v = 0$ state.

5.3 The Structure of ^{205}PbF

A significantly more extreme change to the structure of energy levels in PbF takes the form of switching to ^{205}Pb, an isotope with a nuclear spin of $\frac{5}{2}$ and an additional parameter in the form of the eQq. Along with extra nuclear spin states these factors present additional predictive complexity in comparison with simple vibrational scaling. While this additional complexity can complicate the fitting and prediction of an isotopologue, it also could allow for more opposite parity level mixing and potentially more favorable near-degeneracy.

5.3.1 Scaling ^{205}PbF Parameters

As mentioned previously, when scaling between two isotopes of nonzero nuclear spin, hyperfine paramaters must be scaled according to magnetic moment ratios in addition to isotopic mass ratios. Additionally, parameters scale inversely according to their number of nuclear spin states. To isotopically scale the ^{205}PbF parameters from the ^{207}PbF parameters from the global fit, the relevant magnetic moments were $g_N^{205} = +0.7117(4)$ Bohr magnetons (μ_N) and $g_N^{207} = +0.592583(9)$ μ_N. Dividing the ^{207}PbF magnetic moment by the ^{205}PbF magnetic moment and then dividing by their spin ratio (5) yields the value 4.1632. Dividing each hyperfine parameter by this constant value, in addition to the mass scaling described in Table 3, yields the scaled parameters for the ^{205}PbF prediction.

5.3.2 The Nuclear Quadrupole Moment of ^{205}PbF

As discussed in section 3.1, the nuclear quadrupole effective Hamiltonian takes the form

$$\boldsymbol{H}_{eQq} = eQq(\mathrm{Pb})\frac{3I_z^{(\mathrm{Pb})} - \left(\mathbf{I}^{(\mathrm{Pb})}\right)^2}{4I^{(\mathrm{Pb})}\left(2I^{(\mathrm{Pb})} - 1\right)}. \tag{5.1}$$

In order to implement this parameter into our predictive model, we included a preliminary value obtained from *ab initio* calculations using a Q value of 23.6 fm^2 [43], informed by the recent detailed study of ^{173}YbF [45]. The eQq value obtained for the $^2\Pi_{1/2}$ electronic state from this calculation was -22.5 MHz. This value is surprisingly and significantly different from the $^2\Pi_{3/2}$ result of -220.8 MHz [62]. For comparison, the ^{173}YbF eQq values calculated with similar methods are -3386(78) MHz and -2083(153) MHz for the corresponding X $^2\Sigma^+$ and A $^2\Pi_{1/2}$ states. While these values will be refined with more sophisticated calculations, their current value in conjunction with our preliminary global fit provides a reasonable first estimate at the energy level structure of ^{205}PbF.

5.3.3 Results

Our current analysis focuses only on the ground $^2\Pi_{1/2}$, $v = 0$ state of ^{205}PbF, since our FTMW data for other isotopologues is primarily for these states. The predicted energy level structure for the lowest 24 states can be found plotted in Figure 15 and listed in Table 5. No significant near-degeneracy of states of opposite parity is currently found in our predictions, and as in the ^{207}PbF case, the spacing between energy levels of opposite parity appears to increase with J. Addtionally, varying the calculated eQq value by as much as 50% has little effect on the predicted energy level structure. However, the preliminary nature of these results, arising from both the uncertainty in the calculated eQq value and residual errors in the global fit, indicates that further investigation should definitely be pursued.

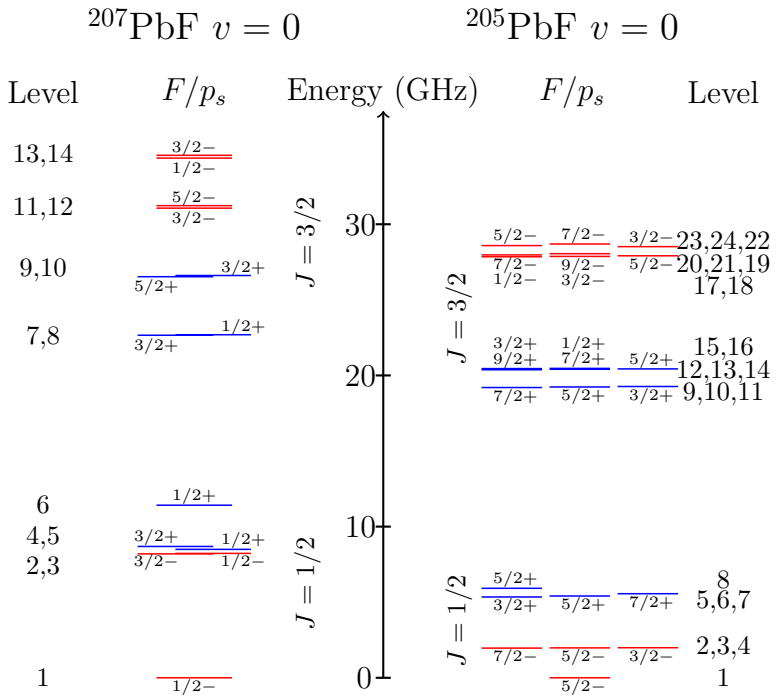

Figure 15: Predicted energy level diagrams of the low-lying $v = 0$ states of ^{207}PbF on the left and ^{205}PbF on the right. Parity has been labeled red/blue for $-/+$ parity, respectively.

Table 5: First 24 Predicted Energy Levels of ^{205}PbF

Level	J	P	F_1	F	Absolute Energy (MHz)
24	1.5	−	4	3.5	28 692.986
23	1.5	−	3	2.5	28 589.228
22	1.5	−	1	1.5	28 518.866
21	1.5	−	4	4.5	28 053.259
20	1.5	−	3	3.5	27 971.925
19	1.5	−	2	2.5	27 913.046
18	1.5	−	2	1.5	27 873.203
17	1.5	−	1	0.5	27 850.119
16	1.5	+	1	0.5	20 465.871
15	1.5	+	2	1.5	20 452.890
14	1.5	+	2	2.5	20 432.235
13	1.5	+	3	3.5	20 405.553
12	1.5	+	4	4.5	20 375.334
11	1.5	+	1	1.5	19 268.140
10	1.5	+	3	2.5	19 236.932
9	1.5	+	4	3.5	19 199.278
8	0.5	+	3	2.5	5 919.372
7	0.5	+	3	3.5	5 562.349
6	0.5	+	2	2.5	5 410.174
5	0.5	+	2	1.5	5 346.049
4	0.5	−	2	1.5	1 989.602
3	0.5	−	2	2.5	1 978.900
2	0.5	−	3	3.5	1 963.880
1	0.5	−	3	2.5	0

6 Conclusion

In this thesis, an overview of the role of diatomic molecules in fundamental physics experiments has been linked to the spectroscopic understanding of these molecules, and a refined global Dunham fit of 83 Fourier-transform microwave transitions (16 new in this work) and 608 Fourier-transform infrared optical transitions has been presented for PbF. This global fit represents one of the most complete descriptions of the molecule, with known rotational, vibrational, and isotopic scaling relationships.

In its current state, the global fit does not quite produce observed minus calculated values within the expected error bars of the observed transitions. There are signs of systematic errors in the fit, including unresolved mass scaling inconsistencies in the low resolution infrared data. Still, reasonable Born-Oppenheimer breakdown terms have been observed for the lowest-order rovibrational parameter (Y_{01}) and the lowest-order Λ-doubling parameter (p_{00}).

Despite isotopic mass scaling errors, this global fit still represents a very significant and broad increase in our knowledge of PbF and serves as a viable platform for predicting a number of interesting states of PbF for parity violation studies. Special attention has been paid to finding energy levels of opposite parity that exhibit more near degeneracy than those recently discovered in the ground state of ^{207}PbF. Preliminary results indicate that the spacing between equivalent levels in the $v = 1$ state of ^{207}PbF is even smaller, while suggesting that the structure of the ground state of ^{205}PbF does not appear to have similar nearly degenerate states.

Further work includes refining the global fit to completely eliminate systematic errors, extending the predictive work on ^{205}PbF, and collecting more vibrational data to explore near-degeneracies in $v = 2$ and higher vibrational states.

A Data

A.1 Fourier-Transform Microwave Data

The $v = 0$ transitions have been previously published [13], while the 16 $v = 1$ transitions are new with this work.

^{208}PbF $^{2}\Pi_{1/2}$

N'	P'	v'	J'	F'	N''	P''	v''	J''	F''	Obs.(MHz)	Unc.(MHz)
1	1	0	0.5	0	1	-1	0	0.5	1	3922.50648	0.0005
1	1	0	0.5	1	1	-1	0	0.5	0	4194.77734	0.0005
1	1	0	0.5	1	1	-1	0	0.5	1	4229.71764	0.0005
2	-1	0	1.5	1	2	1	0	1.5	1	8117.30169	0.0005
2	-1	0	1.5	1	2	1	0	1.5	2	8199.84780	0.0005
2	-1	0	1.5	2	2	1	0	1.5	1	8307.51802	0.0005
2	-1	0	1.5	2	2	1	0	1.5	2	8390.06637	0.0005
3	1	0	2.5	2	3	-1	0	2.5	2	12277.68224	0.0005
3	1	0	2.5	2	3	-1	0	2.5	3	12374.67007	0.0005
3	1	0	2.5	3	3	-1	0	2.5	2	12443.85768	0.0005
3	1	0	2.5	3	3	-1	0	2.5	3	12540.84651	0.0005
4	-1	0	3.5	3	4	1	0	3.5	3	16428.51597	0.0005
4	-1	0	3.5	4	4	1	0	3.5	4	16688.49294	0.0005
2	1	0	1.5	2	1	-1	0	0.5	1	18414.58796	0.0005
2	1	0	1.5	1	1	-1	0	0.5	0	18462.19332	0.0005
2	1	0	1.5	1	1	-1	0	0.5	1	18497.13522	0.0005
2	-1	0	1.5	2	1	1	0	0.5	1	22574.93438	0.0005
2	-1	0	1.5	1	1	1	0	0.5	0	22691.93060	0.0005
2	-1	0	1.5	1	1	1	0	0.5	1	22384.71706	0.0005
2	1	1	1.5	2	1	-1	1	0.5	1	18280.36375[a]	0.0005
2	1	1	1.5	1	1	-1	1	0.5	0	18327.11545[a]	0.0005
2	1	1	1.5	1	1	-1	1	0.5	1	18364.30706[a,b]	0.0007
2	-1	1	1.5	1	1	1	1	0.5	1	22251.82489[a]	0.0005
2	-1	1	1.5	2	1	1	1	0.5	1	22442.64603[a]	0.0005
2	-1	1	1.5	1	1	1	1	0.5	0	22559.29702[a]	0.0005

[a] This work

[b] Larger error due to experimental difficulties

^{207}PbF $^{2}\Pi_{1/2}$

N'	P'	v'	J'	F_1'	F'	N''	P''	v''	J''	F_1''	F''	Obs.(MHz)	Unc.(MHz)
1	1	0	0.5	0	0.5	1	-1	0	0.5	1	0.5	3187.48749	0.0005
1	1	0	0.5	0	0.5	1	-1	0	0.5	1	1.5	3219.81373	0.0005
2	-1	0	1.5	2	1.5	2	1	0	1.5	2	1.5	4455.45403	0.0005
2	-1	0	1.5	2	2.5	2	1	0	1.5	2	2.5	4699.22651	0.0005
1	1	0	0.5	1	0.5	1	-1	0	0.5	0	0.5	8495.00218	0.0005
3	1	0	2.5	3	2.5	3	-1	0	2.5	3	2.5	8620.54753	0.0005
1	1	0	0.5	1	1.5	1	-1	0	0.5	0	0.5	8687.20982	0.0005
2	-1	0	1.5	1	0.5	2	1	0	1.5	1	0.5	11682.52107	0.0005
2	-1	0	1.5	1	0.5	2	1	0	1.5	1	1.5	11715.37030	0.0005
2	-1	0	1.5	1	1.5	2	1	0	1.5	1	0.5	11867.64154	0.0005
2	-1	0	1.5	1	1.5	2	1	0	1.5	1	1.5	11900.48704	0.0005
2	1	0	1.5	1	1.5	1	-1	0	0.5	1	0.5	14430.18298	0.0005
2	1	0	1.5	1	1.5	1	-1	0	0.5	1	1.5	14462.51043	0.0005
2	1	0	1.5	1	0.5	1	-1	0	0.5	1	0.5	14463.03111	0.0005
2	1	0	1.5	1	0.5	1	-1	0	0.5	1	1.5	14495.35797	0.0005
3	1	0	2.5	2	1.5	3	-1	0	2.5	2	1.5	15865.18882	0.0005
3	1	0	2.5	2	2.5	3	-1	0	2.5	2	2.5	16108.72710[a]	0.0005
2	1	0	1.5	2	2.5	1	-1	0	0.5	1	1.5	18333.50131	0.0005
2	1	0	1.5	2	1.5	1	-1	0	0.5	1	0.5	18380.87112	0.0005
2	1	0	1.5	2	1.5	1	-1	0	0.5	1	1.5	18413.19816	0.0005
2	-1	0	1.5	2	1.5	1	1	0	0.5	1	1.5	22377.83416	0.0005
2	-1	0	1.5	2	2.5	1	1	0	0.5	1	1.5	22541.91225	0.0005
2	-1	0	1.5	2	1.5	1	1	0	0.5	1	0.5	22570.04272	0.0005
2	1	0	1.5	1	1.5	1	-1	0	0.5	0	0.5	22658.90179	0.0005
2	1	0	1.5	1	0.5	1	-1	0	0.5	0	0.5	22691.74864	0.0005
2	-1	0	1.5	1	0.5	1	1	0	0.5	0	0.5	22958.06520	0.0005
2	-1	0	1.5	1	1.5	1	1	0	0.5	0	0.5	23143.18458	0.0005
2	-1	0	1.5	1	0.5	1	1	0	0.5	1	1.5	25687.06011	0.0005
2	-1	0	1.5	1	1.5	1	1	0	0.5	1	1.5	25872.17892	0.0005
2	-1	0	1.5	1	0.5	1	1	0	0.5	1	0.5	25879.26671	0.0005
2	-1	0	1.5	1	1.5	1	1	0	0.5	1	0.5	26064.38734	0.0005
2	1	1	1.5	2	2.5	1	-1	1	0.5	1	1.5	18199.42792[b]	0.0005
2	1	1	1.5	2	1.5	1	-1	1	0.5	1	0.5	18246.41532[b]	0.0005
2	-1	1	1.5	2	2.5	1	1	1	0.5	1	1.5	22416.68639[b]	0.0005
2	-1	1	1.5	2	1.5	1	1	1	0.5	1	0.5	22444.02685[b]	0.0005

[a] The fit described in this thesis used the erroneous value of 16108.76330 MHz for this transition. The RMS of the fit with the value listed above is 3.07.

[b] This work

^{206}PbF $^2\Pi_{1/2}$

N'	P'	v'	J'	F'	N''	P''	v''	J''	F''	Obs.(MHz)	Unc.(MHz)
1	1	0	0.5	0	1	-1	0	0.5	1	3925.89105	0.0005
1	1	0	0.5	1	1	-1	0	0.5	0	4198.15987	0.0005
1	1	0	0.5	1	1	-1	0	0.5	1	4233.09109	0.0005
2	-1	0	1.5	1	2	1	0	1.5	1	8124.06457	0.0005
2	-1	0	1.5	1	2	1	0	1.5	2	8206.61122	0.0005
2	-1	0	1.5	2	2	1	0	1.5	1	8314.28438	0.0005
2	-1	0	1.5	2	2	1	0	1.5	2	8396.83017	0.0005
2	1	0	1.5	2	1	-1	0	0.5	1	18429.54268	0.0005
2	1	0	1.5	1	1	-1	0	0.5	0	18477.14786	0.0005
2	1	0	1.5	1	1	-1	0	0.5	1	18512.09022	0.0005
2	-1	0	1.5	2	1	1	0	0.5	1	22593.27178	0.0005
2	-1	0	1.5	1	1	1	0	0.5	0	22710.26738	0.0005
2	1	1	1.5	2	1	-1	1	0.5	1	18295.15526[a]	0.0005
2	1	1	1.5	1	1	-1	1	0.5	0	18341.90629[a]	0.0005
2	1	1	1.5	1	1	-1	1	0.5	1	18379.09805[a,b]	0.0007
2	-1	1	1.5	1	1	1	1	0.5	1	22270.00064[a]	0.0005
2	-1	1	1.5	2	1	1	1	0.5	1	22460.82147[a]	0.0005
2	-1	1	1.5	1	1	1	1	0.5	0	22577.47200[a]	0.0005

[a] This work

[b] Larger error due to experimental difficulties

^{204}PbF $^2\Pi_{1/2}$

N'	P'	v'	J'	F'	N''	P''	v''	J''	F''	Obs.(MHz)	Unc.(MHz)
2	1	0	1.5	1	1	-1	0	0.5	0	18492.39223	0.0005
2	1	0	1.5	1	1	-1	0	0.5	1	18527.33549	0.0005
2	-1	0	1.5	1	1	1	0	0.5	1	22421.74365	0.0005
2	-1	0	1.5	2	1	1	0	0.5	1	22611.96289	0.0005
2	-1	0	1.5	1	1	1	0	0.5	0	22728.95686	0.0005

A.2 Fourier-Transform Infrared Data [14], [63]

All FTIR data presented here is consistent with the smaller published data set.

^{208}PbF $^2\Pi_{3/2} \rightarrow {}^2\Pi_{1/2}$, $v = 0 - 0$

N'	P'	v'	J'	N''	P''	v''	J''	Obs.(cm^{-1})	Unc.(cm^{-1})
2	1	0	2.5	4	-1	0	3.5	8273.9979	0.002
4	1	0	4.5	6	-1	0	5.5	8273.0308	0.002
5	-1	0	5.5	7	1	0	6.5	8272.5637	0.002
6	1	0	6.5	8	-1	0	7.5	8272.1075	0.002
7	-1	0	7.5	9	1	0	8.5	8271.6626	0.002
8	1	0	8.5	10	-1	0	9.5	8271.2263	0.002
10	1	0	10.5	12	-1	0	11.5	8270.3887	0.002
11	-1	0	11.5	13	1	0	12.5	8269.9837	0.002
12	1	0	12.5	14	-1	0	13.5	8269.5905	0.002
13	-1	0	13.5	15	1	0	14.5	8269.2079	0.002
15	-1	0	15.5	17	1	0	16.5	8268.4751	0.002
16	1	0	16.5	18	-1	0	17.5	8268.1246	0.002
17	-1	0	17.5	19	1	0	18.5	8267.7848	0.002
18	1	0	18.5	20	-1	0	19.5	8267.4555	0.002
19	-1	0	19.5	21	1	0	20.5	8267.1369	0.002
20	1	0	20.5	22	-1	0	21.5	8266.8289	0.002
21	-1	0	21.5	23	1	0	22.5	8266.5316	0.002
22	1	0	22.5	24	-1	0	23.5	8266.2449	0.002
23	-1	0	23.5	25	1	0	24.5	8265.9690	0.002
24	1	0	24.5	26	-1	0	25.5	8265.7038	0.002
25	-1	0	25.5	27	1	0	26.5	8265.4494	0.002
26	1	0	26.5	28	-1	0	27.5	8265.2055	0.002
27	-1	0	27.5	29	1	0	28.5	8264.9724	0.002
28	1	0	28.5	30	-1	0	29.5	8264.7493	0.002
29	-1	0	29.5	31	1	0	30.5	8264.5379	0.002
30	1	0	30.5	32	-1	0	31.5	8264.3368	0.002
31	-1	0	31.5	33	1	0	32.5	8264.1467	0.002
32	1	0	32.5	34	-1	0	33.5	8263.9666	0.002
33	-1	0	33.5	35	1	0	34.5	8263.7980	0.002
34	1	0	34.5	36	-1	0	35.5	8263.6398	0.002
35	-1	0	35.5	37	1	0	36.5	8263.4926	0.002
36	1	0	36.5	38	-1	0	37.5	8263.3562	0.002
37	-1	0	37.5	39	1	0	38.5	8263.2303	0.002
38	1	0	38.5	40	-1	0	39.5	8263.1150	0.002
39	-1	0	39.5	41	1	0	40.5	8263.0110	0.002
40	1	0	40.5	42	-1	0	41.5	8262.9171	0.002
41	-1	0	41.5	43	1	0	42.5	8262.8350	0.002
42	1	0	42.5	44	-1	0	43.5	8262.7633	0.002
43	-1	0	43.5	45	1	0	44.5	8262.7035	0.002

^{208}PbF $^2\Pi_{3/2} \rightarrow {}^2\Pi_{1/2}$, $v = 0 - 0$

N'	P'	v'	J'	N''	P''	v''	J''	Obs.(cm^{-1})	Unc.(cm^{-1})
44	1	0	44.5	46	-1	0	45.5	8262.6525	0.002
1	1	0	1.5	3	-1	0	2.5	8274.9100	0.002
2	-1	0	2.5	4	1	0	3.5	8274.5501	0.002
3	1	0	3.5	5	-1	0	4.5	8274.1992	0.002
4	-1	0	4.5	6	1	0	5.5	8273.8597	0.002
5	1	0	5.5	7	-1	0	6.5	8273.5310	0.002
6	-1	0	6.5	8	1	0	7.5	8273.2130	0.002
7	1	0	7.5	9	-1	0	8.5	8272.9055	0.002
8	-1	0	8.5	10	1	0	9.5	8272.6084	0.002
9	1	0	9.5	11	-1	0	10.5	8272.3218	0.002
10	-1	0	10.5	12	1	0	11.5	8272.0460	0.002
11	1	0	11.5	13	-1	0	12.5	8271.7805	0.002
12	-1	0	12.5	14	1	0	13.5	8271.5257	0.002
13	1	0	13.5	15	-1	0	14.5	8271.2817	0.002
14	-1	0	14.5	16	1	0	15.5	8271.0481	0.002
15	1	0	15.5	17	-1	0	16.5	8270.8249	0.002
16	-1	0	16.5	18	1	0	17.5	8270.6131	0.002
17	1	0	17.5	19	-1	0	18.5	8270.4113	0.002
18	-1	0	18.5	20	1	0	19.5	8270.2208	0.002
19	1	0	19.5	21	-1	0	20.5	8270.0401	0.002
20	-1	0	20.5	22	1	0	21.5	8269.8707	0.002
21	1	0	21.5	23	-1	0	22.5	8269.7117	0.002
22	-1	0	22.5	24	1	0	23.5	8269.5643	0.002
23	1	0	23.5	25	-1	0	24.5	8269.4258	0.002
24	-1	0	24.5	26	1	0	25.5	8269.2994	0.002
26	-1	0	26.5	28	1	0	27.5	8269.0777	0.002
27	1	0	27.5	29	-1	0	28.5	8268.9828	0.002
28	-1	0	28.5	30	1	0	29.5	8268.8989	0.002
43	1	0	43.5	45	-1	0	44.5	8268.9331	0.002
44	-1	0	44.5	46	1	0	45.5	8269.0234	0.002
45	1	0	45.5	47	-1	0	46.5	8269.1240	0.002
47	1	0	47.5	49	-1	0	48.5	8269.3549	0.002
48	-1	0	48.5	50	1	0	49.5	8269.4882	0.002
49	1	0	49.5	51	-1	0	50.5	8269.6331	0.002
50	-1	0	50.5	52	1	0	51.5	8269.7860	0.002
52	-1	0	52.5	54	1	0	53.5	8270.1279	0.002
53	1	0	53.5	55	-1	0	54.5	8270.3165	0.002
54	-1	0	54.5	56	1	0	55.5	8270.5142	0.002
24	-1	0	24.5	25	1	0	24.5	8277.3923	0.002

^{208}PbF $^2\Pi_{3/2} \rightarrow {}^2\Pi_{1/2}$, $v = 0 - 0$

N'	P'	v'	J'	N''	P''	v''	J''	Obs.(cm^{-1})	Unc.(cm^{-1})
25	1	0	25.5	26	-1	0	25.5	8277.5924	0.002
26	-1	0	26.5	27	1	0	26.5	8277.8023	0.002
27	1	0	27.5	28	-1	0	27.5	8278.0234	0.002
28	-1	0	28.5	29	1	0	28.5	8278.2548	0.002
29	1	0	29.5	30	-1	0	29.5	8278.4969	0.002
30	-1	0	30.5	31	1	0	30.5	8278.7496	0.002
31	1	0	31.5	32	-1	0	31.5	8279.0131	0.002
32	-1	0	32.5	33	1	0	32.5	8279.2872	0.002
34	-1	0	34.5	35	1	0	34.5	8279.8670	0.002
35	1	0	35.5	36	-1	0	35.5	8280.1729	0.002
36	-1	0	36.5	37	1	0	36.5	8280.4895	0.002
37	1	0	37.5	38	-1	0	37.5	8280.8169	0.002
38	-1	0	38.5	39	1	0	38.5	8281.1545	0.002
39	1	0	39.5	40	-1	0	39.5	8281.5032	0.002
40	-1	0	40.5	41	1	0	40.5	8281.8621	0.002
41	1	0	41.5	42	-1	0	41.5	8282.2318	0.002
42	-1	0	42.5	43	1	0	42.5	8282.6119	0.002
43	1	0	43.5	44	-1	0	43.5	8283.0030	0.002
44	-1	0	44.5	45	1	0	44.5	8283.4050	0.002
45	1	0	45.5	46	-1	0	45.5	8283.8169	0.002
46	-1	0	46.5	47	1	0	46.5	8284.2404	0.002
47	1	0	47.5	48	-1	0	47.5	8284.6741	0.002
48	-1	0	48.5	49	1	0	48.5	8285.1188	0.002
49	1	0	49.5	50	-1	0	49.5	8285.5741	0.002
50	-1	0	50.5	51	1	0	50.5	8286.0399	0.002
51	1	0	51.5	52	-1	0	51.5	8286.5166	0.002
52	-1	0	52.5	53	1	0	52.5	8287.0035	0.002
53	1	0	53.5	54	-1	0	53.5	8287.5020	0.002
54	-1	0	54.5	55	1	0	54.5	8288.0104	0.002
55	1	0	55.5	56	-1	0	55.5	8288.5297	0.002
56	-1	0	56.5	57	1	0	56.5	8289.0613	0.002
58	-1	0	58.5	59	1	0	58.5	8290.1535	0.002
59	1	0	59.5	60	-1	0	59.5	8290.7144	0.002
62	-1	0	62.5	63	1	0	62.5	8292.4683	0.002
63	1	0	63.5	64	-1	0	63.5	8293.0719	0.002
64	-1	0	64.5	65	1	0	64.5	8293.6871	0.002
13	-1	0	13.5	14	1	0	13.5	8277.8246	0.002
14	1	0	14.5	15	-1	0	14.5	8278.0443	0.002
16	1	0	16.5	17	-1	0	16.5	8278.5206	0.002

^{208}PbF $^2\Pi_{3/2} \rightarrow {}^2\Pi_{1/2}$, $v = 0 - 0$

N'	P'	v'	J'	N''	P''	v''	J''	Obs.(cm^{-1})	Unc.(cm^{-1})
17	-1	0	17.5	18	1	0	17.5	8278.7743	0.002
18	1	0	18.5	19	-1	0	18.5	8279.0390	0.002
19	-1	0	19.5	20	1	0	19.5	8279.3137	0.002
20	1	0	20.5	21	-1	0	20.5	8279.5993	0.002
21	-1	0	21.5	22	1	0	21.5	8279.8954	0.002
22	1	0	22.5	23	-1	0	22.5	8280.2020	0.002
23	-1	0	23.5	24	1	0	23.5	8280.5192	0.002
24	1	0	24.5	25	-1	0	24.5	8280.8470	0.002
25	-1	0	25.5	26	1	0	25.5	8281.1854	0.002
26	1	0	26.5	27	-1	0	26.5	8281.5343	0.002
27	-1	0	27.5	28	1	0	27.5	8281.8938	0.002
28	1	0	28.5	29	-1	0	28.5	8282.2641	0.002
30	1	0	30.5	31	-1	0	30.5	8283.0363	0.002
31	-1	0	31.5	32	1	0	31.5	8283.4384	0.002
32	1	0	32.5	33	-1	0	32.5	8283.8512	0.002
33	-1	0	33.5	34	1	0	33.5	8284.2746	0.002
34	1	0	34.5	35	-1	0	34.5	8284.7083	0.002
35	-1	0	35.5	36	1	0	35.5	8285.1529	0.002
36	1	0	36.5	37	-1	0	36.5	8285.6079	0.002
37	-1	0	37.5	38	1	0	37.5	8286.0740	0.002
38	1	0	38.5	39	-1	0	38.5	8286.5505	0.002
39	-1	0	39.5	40	1	0	39.5	8287.0377	0.002
40	1	0	40.5	41	-1	0	40.5	8287.5355	0.002
41	-1	0	41.5	42	1	0	41.5	8288.0439	0.002
42	1	0	42.5	43	-1	0	42.5	8288.5633	0.002
43	-1	0	43.5	44	1	0	43.5	8289.0929	0.002
45	-1	0	45.5	46	1	0	45.5	8290.1848	0.002
46	1	0	46.5	47	-1	0	46.5	8290.7468	0.002
49	-1	0	49.5	50	1	0	49.5	8292.4974	0.002
50	1	0	50.5	51	-1	0	50.5	8293.1021	0.002
51	-1	0	51.5	52	1	0	51.5	8293.7179	0.002
53	-1	0	53.5	54	1	0	53.5	8294.9812	0.002
1	-1	0	1.5	1	1	0	0.5	8276.4580	0.002
3	-1	0	3.5	3	1	0	2.5	8277.2953	0.002
4	1	0	4.5	4	-1	0	3.5	8277.7276	0.002
5	-1	0	5.5	5	1	0	4.5	8278.1749	0.002
6	1	0	6.5	6	-1	0	5.5	8278.6302	0.002
7	-1	0	7.5	7	1	0	6.5	8279.0951	0.002
10	1	0	10.5	10	-1	0	9.5	8280.5564	0.002

^{208}PbF $^2\Pi_{3/2} \rightarrow {}^2\Pi_{1/2}$, $v = 0 - 0$

N'	P'	v'	J'	N''	P''	v''	J''	Obs.(cm^{-1})	Unc.(cm^{-1})
11	-1	0	11.5	11	1	0	10.5	8281.0644	0.002
12	1	0	12.5	12	-1	0	11.5	8281.5831	0.002
13	-1	0	13.5	13	1	0	12.5	8282.1117	0.002
15	-1	0	15.5	15	1	0	14.5	8283.2008	0.002
16	1	0	16.5	16	-1	0	15.5	8283.7614	0.002
17	-1	0	17.5	17	1	0	16.5	8284.3321	0.002
18	1	0	18.5	18	-1	0	17.5	8284.9137	0.002
19	-1	0	19.5	19	1	0	18.5	8285.5055	0.002
20	1	0	20.5	20	-1	0	19.5	8286.1076	0.002
21	-1	0	21.5	21	1	0	20.5	8286.7203	0.002
22	1	0	22.5	22	-1	0	21.5	8287.3438	0.002
23	-1	0	23.5	23	1	0	22.5	8287.9774	0.002
24	1	0	24.5	24	-1	0	23.5	8288.6215	0.002
25	-1	0	25.5	25	1	0	24.5	8289.2763	0.002
26	1	0	26.5	26	-1	0	25.5	8289.9413	0.002
27	-1	0	27.5	27	1	0	26.5	8290.6170	0.002
29	-1	0	29.5	29	1	0	28.5	8291.9993	0.002
30	1	0	30.5	30	-1	0	29.5	8292.7073	0.002
31	-1	0	31.5	31	1	0	30.5	8293.4238	0.002
32	1	0	32.5	32	-1	0	31.5	8294.1517	0.002
33	-1	0	33.5	33	1	0	32.5	8294.8902	0.002
35	-1	0	35.5	35	1	0	34.5	8296.3983	0.002
36	1	0	36.5	36	-1	0	35.5	8297.1675	0.002
37	-1	0	37.5	37	1	0	36.5	8297.9482	0.002
38	1	0	38.5	38	-1	0	37.5	8298.7391	0.002
39	-1	0	39.5	39	1	0	38.5	8299.5399	0.002
41	-1	0	41.5	41	1	0	40.5	8301.1740	0.002
42	1	0	42.5	42	-1	0	41.5	8302.0068	0.002
43	-1	0	43.5	43	1	0	42.5	8302.8492	0.002
44	1	0	44.5	44	-1	0	43.5	8303.7028	0.002
47	-1	0	47.5	47	1	0	46.5	8306.3260	0.002
48	1	0	48.5	48	-1	0	47.5	8307.2214	0.002
49	-1	0	49.5	49	1	0	48.5	8308.1278	0.002
50	1	0	50.5	50	-1	0	49.5	8309.0435	0.002
52	1	0	52.5	52	-1	0	51.5	8310.9103	0.002
53	-1	0	53.5	53	1	0	52.5	8311.8554	0.002
55	-1	0	55.5	55	1	0	54.5	8313.7820	0.002
1	1	0	1.5	1	-1	0	0.5	8276.5978	0.002
2	-1	0	2.5	2	1	0	1.5	8277.1482	0.002

^{208}PbF $^2\Pi_{3/2} \rightarrow {}^2\Pi_{1/2}$, $v = 0 - 0$

N'	P'	v'	J'	N''	P''	v''	J''	Obs.(cm^{-1})	Unc.(cm^{-1})
3	1	0	3.5	3	-1	0	2.5	8277.7117	0.002
5	1	0	5.5	5	-1	0	4.5	8278.8657	0.002
6	-1	0	6.5	6	1	0	5.5	8279.4586	0.002
8	-1	0	8.5	8	1	0	7.5	8280.6781	0.002
9	1	0	9.5	9	-1	0	8.5	8281.3030	0.002
10	-1	0	10.5	10	1	0	9.5	8281.9391	0.002
11	1	0	11.5	11	-1	0	10.5	8282.5858	0.002
12	-1	0	12.5	12	1	0	11.5	8283.2415	0.002
13	1	0	13.5	13	-1	0	12.5	8283.9087	0.002
14	-1	0	14.5	14	1	0	13.5	8284.5864	0.002
15	1	0	15.5	15	-1	0	14.5	8285.2746	0.002
16	-1	0	16.5	16	1	0	15.5	8285.9732	0.002
17	1	0	17.5	17	-1	0	16.5	8286.6825	0.002
18	-1	0	18.5	18	1	0	17.5	8287.4019	0.002
19	1	0	19.5	19	-1	0	18.5	8288.1321	0.002
20	-1	0	20.5	20	1	0	19.5	8288.8728	0.002
22	-1	0	22.5	22	1	0	21.5	8290.3855	0.002
23	1	0	23.5	23	-1	0	22.5	8291.1577	0.002
25	1	0	25.5	25	-1	0	24.5	8292.7332	0.002
26	-1	0	26.5	26	1	0	25.5	8293.5368	0.002
28	-1	0	28.5	28	1	0	27.5	8295.1753	0.002
29	1	0	29.5	29	-1	0	28.5	8296.0098	0.002
30	-1	0	30.5	30	1	0	29.5	8296.8557	0.002
31	1	0	31.5	31	-1	0	30.5	8297.7118	0.002
32	-1	0	32.5	32	1	0	31.5	8298.5782	0.002
33	1	0	33.5	33	-1	0	32.5	8299.4549	0.002
35	1	0	35.5	35	-1	0	34.5	8301.2401	0.002
36	-1	0	36.5	36	1	0	35.5	8302.1482	0.002
37	1	0	37.5	37	-1	0	36.5	8303.0679	0.002
38	-1	0	38.5	38	1	0	37.5	8303.9968	0.002
39	1	0	39.5	39	-1	0	38.5	8304.9368	0.002
40	-1	0	40.5	40	1	0	39.5	8305.8869	0.002
41	1	0	41.5	41	-1	0	40.5	8306.8479	0.002
42	-1	0	42.5	42	1	0	41.5	8307.8193	0.002
43	1	0	43.5	43	-1	0	42.5	8308.8008	0.002
46	-1	0	46.5	46	1	0	45.5	8311.8087	0.002

^{208}PbF $^2\Pi_{3/2} \rightarrow {}^2\Pi_{1/2}$, $v = 1 - 1$

N'	P'	v'	J'	N''	P''	v''	J''	Obs.(cm^{-1})	Unc.(cm^{-1})
3	-1	1	3.5	4	1	1	3.5	8302.232	0.002
4	1	1	4.5	5	-1	1	4.5	8302.349	0.002
5	-1	1	5.5	6	1	1	5.5	8302.477	0.002
7	-1	1	7.5	8	1	1	7.5	8302.763	0.002
8	1	1	8.5	9	-1	1	8.5	8302.922	0.002
2	-1	1	2.5	2	1	1	1.5	8303.192	0.002
10	1	1	10.5	11	-1	1	10.5	8303.272	0.002
11	-1	1	11.5	12	1	1	11.5	8303.465	0.002
12	1	1	12.5	13	-1	1	12.5	8303.666	0.002
4	1	1	4.5	4	-1	1	3.5	8303.762	0.002
13	-1	1	13.5	14	1	1	13.5	8303.878	0.002
4	-1	1	4.5	4	1	1	3.5	8304.334	0.002
6	1	1	6.5	6	-1	1	5.5	8304.662	0.002
17	-1	1	17.5	18	1	1	17.5	8304.834	0.002
18	1	1	18.5	19	-1	1	18.5	8305.101	0.002
32	-1	1	32.5	33	1	1	32.5	8305.317	0.002
19	-1	1	19.5	20	1	1	19.5	8305.377	0.002
6	-1	1	6.5	6	1	1	5.5	8305.495	0.002
8	1	1	8.5	8	-1	1	7.5	8305.599	0.002
20	1	1	20.5	21	-1	1	20.5	8305.663	0.002
7	1	1	7.5	7	-1	1	6.5	8306.088	0.002
22	1	1	22.5	23	-1	1	22.5	8306.270	0.002

^{207}PbF $^2\Pi_{3/2} \rightarrow {}^2\Pi_{1/2}$, $v = 0 - 0$

N'	P'	v'	J'	F_1'	N''	P''	v''	J''	F_1''	Obs.(cm^{-1})	Unc.(cm^{-1})
6	1	0	6.5	7	8	-1	0	7.5	8	8272.1753	0.002
6	1	0	6.5	6	8	-1	0	7.5	7	8272.0533	0.002
8	1	0	8.5	9	10	-1	0	9.5	10	8271.2933	0.002
8	1	0	8.5	8	10	-1	0	9.5	9	8271.1729	0.002
15	-1	0	15.5	15	17	1	0	16.5	16	8268.4206	0.002
16	1	0	16.5	17	18	-1	0	17.5	18	8268.1915	0.002
16	1	0	16.5	16	18	-1	0	17.5	17	8268.0701	0.002
17	-1	0	17.5	18	19	1	0	18.5	19	8267.8515	0.002
17	-1	0	17.5	17	19	1	0	18.5	18	8267.7302	0.002
18	1	0	18.5	19	20	-1	0	19.5	20	8267.5219	0.002
18	1	0	18.5	18	20	-1	0	19.5	19	8267.4005	0.002
19	-1	0	19.5	20	21	1	0	20.5	21	8267.2032	0.002
19	-1	0	19.5	19	21	1	0	20.5	20	8267.0817	0.002
20	1	0	20.5	21	22	-1	0	21.5	22	8266.8952	0.002
20	1	0	20.5	20	22	-1	0	21.5	21	8266.7737	0.002
21	-1	0	21.5	22	23	1	0	22.5	23	8266.5977	0.002
21	-1	0	21.5	21	23	1	0	22.5	22	8266.4764	0.002
22	1	0	22.5	23	24	-1	0	23.5	24	8266.3112	0.002
22	1	0	22.5	22	24	-1	0	23.5	23	8266.1897	0.002
23	-1	0	23.5	24	25	1	0	24.5	25	8266.0350	0.002
23	-1	0	23.5	23	25	1	0	24.5	24	8265.9137	0.002
24	1	0	24.5	25	26	-1	0	25.5	26	8265.7696	0.002
24	1	0	24.5	24	26	-1	0	25.5	25	8265.6485	0.002
25	-1	0	25.5	26	27	1	0	26.5	27	8265.5150	0.002
25	-1	0	25.5	25	27	1	0	26.5	26	8265.3939	0.002
26	1	0	26.5	27	28	-1	0	27.5	28	8265.2710	0.002
26	1	0	26.5	26	28	-1	0	27.5	27	8265.1497	0.002
27	-1	0	27.5	28	29	1	0	28.5	29	8265.0377	0.002
27	-1	0	27.5	27	29	1	0	28.5	28	8264.9163	0.002
28	1	0	28.5	29	30	-1	0	29.5	30	8264.8151	0.002
28	1	0	28.5	28	30	-1	0	29.5	29	8264.6938	0.002
29	-1	0	29.5	30	31	1	0	30.5	31	8264.6032	0.002
29	-1	0	29.5	29	31	1	0	30.5	30	8264.4818	0.002
30	1	0	30.5	31	32	-1	0	31.5	32	8264.4019	0.002
30	1	0	30.5	30	32	-1	0	31.5	31	8264.2805	0.002
31	-1	0	31.5	32	33	1	0	32.5	33	8264.2114	0.002
31	-1	0	31.5	31	33	1	0	32.5	32	8264.0899	0.002
32	1	0	32.5	33	34	-1	0	33.5	34	8264.0319	0.002
6	-1	0	6.5	6	8	1	0	7.5	7	8273.2812	0.002

^{207}PbF $^2\Pi_{3/2} \rightarrow {}^2\Pi_{1/2}$, $v = 0 - 0$

N'	P'	v'	J'	F_1'	N''	P''	v''	J''	F_1''	Obs.(cm^{-1})	Unc.(cm^{-1})
6	-1	0	6.5	7	8	1	0	7.5	8	8273.1609	0.002
7	1	0	7.5	8	9	-1	0	8.5	9	8272.8535	0.002
8	-1	0	8.5	8	10	1	0	9.5	9	8272.6763	0.002
8	-1	0	8.5	9	10	1	0	9.5	10	8272.5572	0.002
9	1	0	9.5	9	11	-1	0	10.5	10	8272.3895	0.002
9	1	0	9.5	10	11	-1	0	10.5	11	8272.2700	0.002
10	-1	0	10.5	10	12	1	0	11.5	11	8272.1132	0.002
10	-1	0	10.5	11	12	1	0	11.5	12	8271.9936	0.002
11	1	0	11.5	11	13	-1	0	12.5	12	8271.8482	0.002
12	-1	0	12.5	13	14	1	0	13.5	14	8271.4734	0.002
13	1	0	13.5	13	15	-1	0	14.5	14	8271.3498	0.002
13	1	0	13.5	14	15	-1	0	14.5	15	8271.2290	0.002
14	-1	0	14.5	14	16	1	0	15.5	15	8271.1164	0.002
14	-1	0	14.5	15	16	1	0	15.5	16	8270.9952	0.002
16	-1	0	16.5	16	18	1	0	17.5	17	8270.6794	0.002
16	-1	0	16.5	17	18	1	0	17.5	18	8270.5597	0.002
18	-1	0	18.5	18	20	1	0	19.5	19	8270.2877	0.002
18	-1	0	18.5	19	20	1	0	19.5	20	8270.1669	0.002
19	1	0	19.5	19	21	-1	0	20.5	20	8270.1074	0.002
34	-1	0	34.5	34	35	1	0	34.5	34	8279.8175	0.002
34	-1	0	34.5	35	35	1	0	34.5	35	8279.9391	0.002
35	1	0	35.5	36	36	-1	0	35.5	36	8280.2449	0.002
36	-1	0	36.5	36	37	1	0	36.5	36	8280.4400	0.002
36	-1	0	36.5	37	37	1	0	36.5	37	8280.5612	0.002
37	1	0	37.5	38	38	-1	0	37.5	38	8280.8890	0.002
38	-1	0	38.5	38	39	1	0	38.5	38	8281.1057	0.002
38	-1	0	38.5	39	39	1	0	38.5	39	8281.2279	0.002
39	1	0	39.5	39	40	-1	0	39.5	39	8281.4538	0.002
39	1	0	39.5	40	40	-1	0	39.5	40	8281.5762	0.002
40	-1	0	40.5	40	41	1	0	40.5	40	8281.8134	0.002
40	-1	0	40.5	41	41	1	0	40.5	41	8281.9356	0.002
41	1	0	41.5	42	42	-1	0	41.5	42	8282.3045	0.002
43	1	0	43.5	43	44	-1	0	43.5	43	8282.9546	0.002
43	1	0	43.5	44	44	-1	0	43.5	44	8283.0759	0.002
44	-1	0	44.5	44	45	1	0	44.5	44	8283.3569	0.002
44	-1	0	44.5	45	45	1	0	44.5	45	8283.4778	0.002
46	-1	0	46.5	46	47	1	0	46.5	46	8284.1927	0.002
47	1	0	47.5	48	48	-1	0	47.5	48	8284.7478	0.002
48	-1	0	48.5	48	49	1	0	48.5	48	8285.0708	0.002

^{207}PbF $^2\Pi_{3/2} \rightarrow {}^2\Pi_{1/2}$, $v = 0 - 0$

N'	P'	v'	J'	F_1'	N''	P''	v''	J''	F_1''	Obs.(cm^{-1})	Unc.(cm^{-1})
49	1	0	49.5	49	50	-1	0	49.5	49	8285.5269	0.002
49	1	0	49.5	50	50	-1	0	49.5	50	8285.6476	0.002
50	-1	0	50.5	50	51	1	0	50.5	50	8285.9922	0.002
52	-1	0	52.5	52	53	1	0	52.5	52	8286.9573	0.002
52	-1	0	52.5	53	53	1	0	52.5	53	8287.0777	0.002
17	-1	0	17.5	17	18	1	0	17.5	17	8278.8450	0.002
18	1	0	18.5	19	19	-1	0	18.5	19	8278.9887	0.002
18	1	0	18.5	18	19	-1	0	18.5	18	8279.1092	0.002
19	-1	0	19.5	20	20	1	0	19.5	20	8279.2640	0.002
19	-1	0	19.5	19	20	1	0	19.5	19	8279.3852	0.002
20	1	0	20.5	21	21	-1	0	20.5	21	8279.5488	0.002
20	1	0	20.5	20	21	-1	0	20.5	20	8279.6701	0.002
21	-1	0	21.5	22	22	1	0	21.5	22	8279.8459	0.002
21	-1	0	21.5	21	22	1	0	21.5	21	8279.9664	0.002
22	1	0	22.5	22	23	-1	0	22.5	22	8280.2732	0.002
23	-1	0	23.5	24	24	1	0	23.5	24	8280.4699	0.002
23	-1	0	23.5	23	24	1	0	23.5	23	8280.5904	0.002
24	1	0	24.5	25	25	-1	0	24.5	25	8280.7979	0.002
24	1	0	24.5	24	25	-1	0	24.5	24	8280.9186	0.002
26	1	0	26.5	27	27	-1	0	26.5	27	8281.4854	0.002
26	1	0	26.5	26	27	-1	0	26.5	26	8281.6059	0.002
27	-1	0	27.5	28	28	1	0	27.5	28	8281.8451	0.002
27	-1	0	27.5	27	28	1	0	27.5	27	8281.9657	0.002
28	1	0	28.5	29	29	-1	0	28.5	29	8282.2155	0.002
28	1	0	28.5	28	29	-1	0	28.5	28	8282.3363	0.002
30	1	0	30.5	31	31	-1	0	30.5	31	8282.9881	0.002
30	1	0	30.5	30	31	-1	0	30.5	30	8283.1088	0.002
31	-1	0	31.5	32	32	1	0	31.5	32	8283.3904	0.002
31	-1	0	31.5	31	32	1	0	31.5	31	8283.5109	0.002
32	1	0	32.5	33	33	-1	0	32.5	33	8283.8036	0.002
32	1	0	32.5	32	33	-1	0	32.5	32	8283.9237	0.002
33	-1	0	33.5	34	34	1	0	33.5	34	8284.2268	0.002
33	-1	0	33.5	33	34	1	0	33.5	33	8284.3472	0.002
34	1	0	34.5	34	35	-1	0	34.5	34	8284.7815	0.002
35	-1	0	35.5	36	36	1	0	35.5	36	8285.1053	0.002
37	-1	0	37.5	38	38	1	0	37.5	38	8286.0307	0.002
37	-1	0	37.5	37	38	1	0	37.5	37	8286.1479	0.002
38	1	0	38.5	39	39	-1	0	38.5	39	8286.5035	0.002
39	-1	0	39.5	40	40	1	0	39.5	40	8286.9909	0.002

^{207}PbF $^2\Pi_{3/2} \rightarrow {}^2\Pi_{1/2}$, $v = 0 - 0$

N'	P'	v'	J'	F_1'	N''	P''	v''	J''	F_1''	Obs.(cm^{-1})	Unc.(cm^{-1})
39	-1	0	39.5	39	40	1	0	39.5	39	8287.1118	0.002
40	1	0	40.5	40	41	-1	0	40.5	40	8287.6098	0.002
42	1	0	42.5	42	43	-1	0	42.5	42	8288.6376	0.002
43	-1	0	43.5	44	44	1	0	43.5	44	8289.0471	0.002
43	-1	0	43.5	43	44	1	0	43.5	43	8289.1683	0.002
45	-1	0	45.5	46	46	1	0	45.5	46	8290.1396	0.002
45	-1	0	45.5	45	46	1	0	45.5	45	8290.2607	0.002
46	1	0	46.5	46	47	-1	0	46.5	46	8290.8228	0.002
48	1	0	48.5	49	49	-1	0	48.5	49	8291.8585	0.002
49	-1	0	49.5	50	50	1	0	49.5	50	8292.4527	0.002
49	-1	0	49.5	49	50	1	0	49.5	49	8292.5740	0.002
50	1	0	50.5	51	51	-1	0	50.5	51	8293.0577	0.002
11	-1	0	11.5	11	11	1	0	10.5	10	8281.0152	0.002
12	1	0	12.5	12	12	-1	0	11.5	11	8281.5341	0.002
12	1	0	12.5	13	12	-1	0	11.5	12	8281.6555	0.002
13	-1	0	13.5	13	13	1	0	12.5	12	8282.0631	0.002
15	-1	0	15.5	15	15	1	0	14.5	14	8283.1527	0.002
15	-1	0	15.5	16	15	1	0	14.5	15	8283.2736	0.002
16	1	0	16.5	16	16	-1	0	15.5	15	8283.7131	0.002
16	1	0	16.5	17	16	-1	0	15.5	16	8283.8362	0.002
17	-1	0	17.5	17	17	1	0	16.5	16	8284.2832	0.002
17	-1	0	17.5	18	17	1	0	16.5	17	8284.4054	0.002
18	1	0	18.5	18	18	-1	0	17.5	17	8284.8658	0.002
18	1	0	18.5	19	18	-1	0	17.5	18	8284.9873	0.002
19	-1	0	19.5	19	19	1	0	18.5	18	8285.4579	0.002
20	1	0	20.5	21	20	-1	0	19.5	20	8286.1818	0.002
21	-1	0	21.5	21	21	1	0	20.5	20	8286.6745	0.002
21	-1	0	21.5	22	21	1	0	20.5	21	8286.7948	0.002
22	1	0	22.5	22	22	-1	0	21.5	21	8287.2972	0.002
22	1	0	22.5	23	22	-1	0	21.5	22	8287.4181	0.002
23	-1	0	23.5	23	23	1	0	22.5	22	8287.9309	0.002
23	-1	0	23.5	24	23	1	0	22.5	23	8288.0515	0.002
24	1	0	24.5	24	24	-1	0	23.5	23	8288.5747	0.002
24	1	0	24.5	25	24	-1	0	23.5	24	8288.6966	0.002
25	-1	0	25.5	25	25	1	0	24.5	24	8289.2300	0.002
25	-1	0	25.5	26	25	1	0	24.5	25	8289.3516	0.002
26	1	0	26.5	26	26	-1	0	25.5	25	8289.8958	0.002
26	1	0	26.5	27	26	-1	0	25.5	26	8290.0170	0.002
27	-1	0	27.5	27	27	1	0	26.5	26	8290.5717	0.002

^{207}PbF $^2\Pi_{3/2} \rightarrow {}^2\Pi_{1/2}$, $v = 0 - 0$

N'	P'	v'	J'	F_1'	N''	P''	v''	J''	F_1''	Obs.(cm^{-1})	Unc.(cm^{-1})
29	-1	0	29.5	30	29	1	0	28.5	29	8292.0754	0.002
30	1	0	30.5	30	30	-1	0	29.5	29	8292.6632	0.002
30	1	0	30.5	31	30	-1	0	29.5	30	8292.7845	0.002
31	-1	0	31.5	31	31	1	0	30.5	30	8293.3797	0.002
32	1	0	32.5	32	32	-1	0	31.5	31	8294.1076	0.002
33	-1	0	33.5	33	33	1	0	32.5	32	8294.8463	0.002
33	-1	0	33.5	34	33	1	0	32.5	33	8294.9682	0.002
34	1	0	34.5	34	34	-1	0	33.5	33	8295.5925	0.002
34	1	0	34.5	35	34	-1	0	33.5	34	8295.7143	0.002
35	-1	0	35.5	35	35	1	0	34.5	34	8296.3569	0.002
35	-1	0	35.5	36	35	1	0	34.5	35	8296.4771	0.002
36	1	0	36.5	36	36	-1	0	35.5	35	8297.1248	0.002
36	1	0	36.5	37	36	-1	0	35.5	36	8297.2467	0.002
37	-1	0	37.5	37	37	1	0	36.5	36	8297.9055	0.002
37	-1	0	37.5	38	37	1	0	36.5	37	8298.0272	0.002
38	1	0	38.5	38	38	-1	0	37.5	37	8298.6969	0.002
38	1	0	38.5	39	38	-1	0	37.5	38	8298.8182	0.002
39	-1	0	39.5	39	39	1	0	38.5	38	8299.4978	0.002
39	-1	0	39.5	40	39	1	0	38.5	39	8299.6199	0.002
41	-1	0	41.5	41	41	1	0	40.5	40	8301.1327	0.002
41	-1	0	41.5	42	41	1	0	40.5	41	8301.2529	0.002
9	1	0	9.5	9	9	-1	0	8.5	8	8281.3743	0.002
10	-1	0	10.5	10	10	1	0	9.5	9	8282.0110	0.002
11	1	0	11.5	12	11	-1	0	10.5	11	8282.5367	0.002
12	-1	0	12.5	13	12	1	0	11.5	12	8283.1943	0.002
12	-1	0	12.5	12	12	1	0	11.5	11	8283.3139	0.002
13	1	0	13.5	13	13	-1	0	12.5	12	8283.9813	0.002
14	-1	0	14.5	15	14	1	0	13.5	14	8284.5383	0.002
15	1	0	15.5	15	15	-1	0	14.5	14	8285.3479	0.002
16	-1	0	16.5	17	16	1	0	15.5	16	8285.9259	0.002
17	1	0	17.5	17	17	-1	0	16.5	16	8286.7558	0.002
18	-1	0	18.5	19	18	1	0	17.5	18	8287.3542	0.002
20	-1	0	20.5	21	20	1	0	19.5	20	8288.8266	0.002
20	-1	0	20.5	20	20	1	0	19.5	19	8288.9480	0.002
21	1	0	21.5	22	21	-1	0	20.5	21	8289.5816	0.002
22	-1	0	22.5	23	22	1	0	21.5	22	8290.3400	0.002
22	-1	0	22.5	22	22	1	0	21.5	21	8290.4609	0.002
23	1	0	23.5	24	23	-1	0	22.5	23	8291.1124	0.002
24	-1	0	24.5	25	24	1	0	23.5	24	8291.8959	0.002

^{207}PbF $^2\Pi_{3/2} \rightarrow {}^2\Pi_{1/2}$, $v = 0 - 0$

N'	P'	v'	J'	F_1'	N''	P''	v''	J''	F_1''	Obs.(cm^{-1})	Unc.(cm^{-1})
24	-1	0	24.5	24	24	1	0	23.5	23	8292.0158	0.002
25	1	0	25.5	26	25	-1	0	24.5	25	8292.6889	0.002
25	1	0	25.5	25	25	-1	0	24.5	24	8292.8095	0.002
26	-1	0	26.5	26	26	1	0	25.5	25	8293.6135	0.002
29	1	0	29.5	30	29	-1	0	28.5	29	8295.9666	0.002
29	1	0	29.5	29	29	-1	0	28.5	28	8296.0875	0.002
30	-1	0	30.5	31	30	1	0	29.5	30	8296.8125	0.002
30	-1	0	30.5	30	30	1	0	29.5	29	8296.9333	0.002
31	1	0	31.5	32	31	-1	0	30.5	31	8297.6690	0.002
31	1	0	31.5	31	31	-1	0	30.5	30	8297.7899	0.002
32	-1	0	32.5	33	32	1	0	31.5	32	8298.5357	0.002
32	-1	0	32.5	32	32	1	0	31.5	31	8298.6565	0.002
33	1	0	33.5	34	33	-1	0	32.5	33	8299.4131	0.002
33	1	0	33.5	33	33	-1	0	32.5	32	8299.5346	0.002
35	1	0	35.5	36	35	-1	0	34.5	35	8301.1995	0.002
35	1	0	35.5	35	35	-1	0	34.5	34	8301.3200	0.002
36	-1	0	36.5	36	36	1	0	35.5	35	8302.2290	0.002

^{207}PbF $^2\Pi_{3/2} \rightarrow {}^2\Pi_{1/2}$, $v = 1 - 1$

N'	P'	v'	J'	F_1'	N''	P''	v''	J''	F_1''	Obs.(cm^{-1})	Unc.(cm^{-1})
26	1	1	26.5	27	28	-1	1	27.5	28	8291.433	0.002
25	-1	1	25.5	25	27	1	1	26.5	26	8291.550	0.002
25	-1	1	25.5	26	27	1	1	26.5	27	8291.672	0.002
23	-1	1	23.5	24	25	1	1	24.5	25	8292.184	0.002
21	-1	1	21.5	21	23	1	1	22.5	22	8292.613	0.002
21	-1	1	21.5	22	23	1	1	22.5	23	8292.741	0.002
20	1	1	20.5	20	22	-1	1	21.5	21	8292.910	0.002
19	-1	1	19.5	19	21	1	1	20.5	20	8293.213	0.002
19	-1	1	19.5	20	21	1	1	20.5	21	8293.334	0.002
17	-1	1	17.5	17	19	1	1	18.5	18	8293.849	0.002
17	-1	1	17.5	18	19	1	1	18.5	19	8293.972	0.002
15	-1	1	15.5	15	17	1	1	16.5	16	8294.534	0.002
15	-1	1	15.5	16	17	1	1	16.5	17	8294.656	0.002
33	1	1	33.5	34	33	-1	1	32.5	33	8325.410	0.002
39	-1	1	39.5	39	39	1	1	38.5	38	8325.490	0.002
33	1	1	33.5	33	33	-1	1	32.5	32	8325.530	0.002
39	-1	1	39.5	40	39	1	1	38.5	39	8325.611	0.002
34	-1	1	34.5	35	34	1	1	33.5	34	8326.301	0.002
34	-1	1	34.5	34	34	1	1	33.5	33	8326.419	0.002
38	-1	1	38.5	39	38	1	1	37.5	38	8329.949	0.002
38	-1	1	38.5	38	38	1	1	37.5	37	8330.069	0.002
39	1	1	39.5	40	39	-1	1	38.5	39	8330.890	0.002
39	1	1	39.5	39	39	-1	1	38.5	38	8331.011	0.002
34	1	1	34.5	34	34	-1	1	33.5	33	8321.588	0.002
54	1	1	54.5	55	55	-1	1	54.5	55	8321.613	0.002
34	1	1	34.5	35	34	-1	1	33.5	34	8321.712	0.002
54	1	1	54.5	54	55	-1	1	54.5	54	8321.747	0.002

^{206}PbF $^2\Pi_{3/2} \rightarrow {}^2\Pi_{1/2}$, $v = 0 - 0$

N'	P'	v'	J'	N''	P''	v''	J''	Obs.(cm^{-1})	Unc.(cm^{-1})
4	1	0	4.5	6	-1	0	5.5	8273.0442	0.002
5	-1	0	5.5	7	1	0	6.5	8272.5775	0.002
6	1	0	6.5	8	-1	0	7.5	8272.1197	0.002
7	-1	0	7.5	9	1	0	8.5	8271.6745	0.002
8	1	0	8.5	10	-1	0	9.5	8271.2385	0.002
11	-1	0	11.5	13	1	0	12.5	8269.9946	0.002
12	1	0	12.5	14	-1	0	13.5	8269.6005	0.002
13	-1	0	13.5	15	1	0	14.5	8269.2171	0.002
15	-1	0	15.5	17	1	0	16.5	8268.4849	0.002
16	1	0	16.5	18	-1	0	17.5	8268.1341	0.002
17	-1	0	17.5	19	1	0	18.5	8267.7938	0.002
18	1	0	18.5	20	-1	0	19.5	8267.4644	0.002
19	-1	0	19.5	21	1	0	20.5	8267.1453	0.002
20	1	0	20.5	22	-1	0	21.5	8266.8370	0.002
21	-1	0	21.5	23	1	0	22.5	8266.5395	0.002
22	1	0	22.5	24	-1	0	23.5	8266.2525	0.002
23	-1	0	23.5	25	1	0	24.5	8265.9763	0.002
24	1	0	24.5	26	-1	0	25.5	8265.7110	0.002
25	-1	0	25.5	27	1	0	26.5	8265.4561	0.002
26	1	0	26.5	28	-1	0	27.5	8265.2123	0.002
27	-1	0	27.5	29	1	0	28.5	8264.9788	0.002
28	1	0	28.5	30	-1	0	29.5	8264.7562	0.002
29	-1	0	29.5	31	1	0	30.5	8264.5442	0.002
30	1	0	30.5	32	-1	0	31.5	8264.3429	0.002
31	-1	0	31.5	33	1	0	32.5	8264.1524	0.002
32	1	0	32.5	34	-1	0	33.5	8263.9728	0.002
33	-1	0	33.5	35	1	0	34.5	8263.8039	0.002
34	1	0	34.5	36	-1	0	35.5	8263.6454	0.002
35	-1	0	35.5	37	1	0	36.5	8263.4981	0.002
36	1	0	36.5	38	-1	0	37.5	8263.3609	0.002
37	-1	0	37.5	39	1	0	38.5	8263.2354	0.002
38	1	0	38.5	40	-1	0	39.5	8263.1205	0.002
39	-1	0	39.5	41	1	0	40.5	8263.0166	0.002
40	1	0	40.5	42	-1	0	41.5	8262.9228	0.002
41	-1	0	41.5	43	1	0	42.5	8262.8400	0.002
42	1	0	42.5	44	-1	0	43.5	8262.7680	0.002
3	1	0	3.5	5	-1	0	4.5	8274.2132	0.002
4	-1	0	4.5	6	1	0	5.5	8273.8733	0.002
5	1	0	5.5	7	-1	0	6.5	8273.5440	0.002

^{206}PbF $^2\Pi_{3/2} \rightarrow {}^2\Pi_{1/2}$, $v = 0 - 0$

N'	P'	v'	J'	N''	P''	v''	J''	Obs.(cm^{-1})	Unc.(cm^{-1})
6	-1	0	6.5	8	1	0	7.5	8273.2264	0.002
7	1	0	7.5	9	-1	0	8.5	8272.9186	0.002
8	-1	0	8.5	10	1	0	9.5	8272.6212	0.002
9	1	0	9.5	11	-1	0	10.5	8272.3337	0.002
10	-1	0	10.5	12	1	0	11.5	8272.0582	0.002
11	1	0	11.5	13	-1	0	12.5	8271.7927	0.002
12	-1	0	12.5	14	1	0	13.5	8271.5373	0.002
13	1	0	13.5	15	-1	0	14.5	8271.2933	0.002
14	-1	0	14.5	16	1	0	15.5	8271.0596	0.002
15	1	0	15.5	17	-1	0	16.5	8270.8359	0.002
16	-1	0	16.5	18	1	0	17.5	8270.6245	0.002
17	1	0	17.5	19	-1	0	18.5	8270.4222	0.002
18	-1	0	18.5	20	1	0	19.5	8270.2316	0.002
19	1	0	19.5	21	-1	0	20.5	8270.0507	0.002
20	-1	0	20.5	22	1	0	21.5	8269.8813	0.002
21	1	0	21.5	23	-1	0	22.5	8269.7224	0.002
22	-1	0	22.5	24	1	0	23.5	8269.5746	0.002
23	1	0	23.5	25	-1	0	24.5	8269.4362	0.002
24	-1	0	24.5	26	1	0	25.5	8269.3094	0.002
26	-1	0	26.5	28	1	0	27.5	8269.0879	0.002
27	1	0	27.5	29	-1	0	28.5	8268.9929	0.002
28	-1	0	28.5	30	1	0	29.5	8268.9087	0.002
30	-1	0	30.5	32	1	0	31.5	8268.7725	0.002
41	1	0	41.5	43	-1	0	42.5	8268.7984	0.002
43	1	0	43.5	45	-1	0	44.5	8268.9437	0.002
44	-1	0	44.5	46	1	0	45.5	8269.0336	0.002
45	1	0	45.5	47	-1	0	46.5	8269.1326	0.002
46	-1	0	46.5	48	1	0	47.5	8269.2438	0.002
47	1	0	47.5	49	-1	0	48.5	8269.3647	0.002
49	1	0	49.5	51	-1	0	50.5	8269.6436	0.002
50	-1	0	50.5	52	1	0	51.5	8269.7984	0.002
51	1	0	51.5	53	-1	0	52.5	8269.9639	0.002
52	-1	0	52.5	54	1	0	53.5	8270.1391	0.002
53	1	0	53.5	55	-1	0	54.5	8270.3270	0.002
27	1	0	27.5	28	-1	0	27.5	8278.0405	0.002
28	-1	0	28.5	29	1	0	28.5	8278.2720	0.002
29	1	0	29.5	30	-1	0	29.5	8278.5140	0.002
30	-1	0	30.5	31	1	0	30.5	8278.7674	0.002
31	1	0	31.5	32	-1	0	31.5	8279.0306	0.002

^{206}PbF $^2\Pi_{3/2} \rightarrow {}^2\Pi_{1/2}$, $v = 0 - 0$

N'	P'	v'	J'	N''	P''	v''	J''	Obs.(cm^{-1})	Unc.(cm^{-1})
32	-1	0	32.5	33	1	0	32.5	8279.3049	0.002
34	-1	0	34.5	35	1	0	34.5	8279.8851	0.002
35	1	0	35.5	36	-1	0	35.5	8280.1914	0.002
36	-1	0	36.5	37	1	0	36.5	8280.5080	0.002
37	1	0	37.5	38	-1	0	37.5	8280.8360	0.002
38	-1	0	38.5	39	1	0	38.5	8281.1735	0.002
39	1	0	39.5	40	-1	0	39.5	8281.5224	0.002
40	-1	0	40.5	41	1	0	40.5	8281.8814	0.002
41	1	0	41.5	42	-1	0	41.5	8282.2517	0.002
42	-1	0	42.5	43	1	0	42.5	8282.6312	0.002
43	1	0	43.5	44	-1	0	43.5	8283.0238	0.002
44	-1	0	44.5	45	1	0	44.5	8283.4255	0.002
45	1	0	45.5	46	-1	0	45.5	8283.8380	0.002
46	-1	0	46.5	47	1	0	46.5	8284.2617	0.002
47	1	0	47.5	48	-1	0	47.5	8284.6957	0.002
48	-1	0	48.5	49	1	0	48.5	8285.1401	0.002
49	1	0	49.5	50	-1	0	49.5	8285.5968	0.002
50	-1	0	50.5	51	1	0	50.5	8286.0626	0.002
51	1	0	51.5	52	-1	0	51.5	8286.5396	0.002
52	-1	0	52.5	53	1	0	52.5	8287.0268	0.002
53	1	0	53.5	54	-1	0	53.5	8287.5249	0.002
54	-1	0	54.5	55	1	0	54.5	8288.0333	0.002
55	1	0	55.5	56	-1	0	55.5	8288.5534	0.002
16	1	0	16.5	17	-1	0	16.5	8278.5378	0.002
17	-1	0	17.5	18	1	0	17.5	8278.7916	0.002
18	1	0	18.5	19	-1	0	18.5	8279.0566	0.002
19	-1	0	19.5	20	1	0	19.5	8279.3316	0.002
20	1	0	20.5	21	-1	0	20.5	8279.6173	0.002
21	-1	0	21.5	22	1	0	21.5	8279.9138	0.002
22	1	0	22.5	23	-1	0	22.5	8280.2207	0.002
23	-1	0	23.5	24	1	0	23.5	8280.5382	0.002
24	1	0	24.5	25	-1	0	24.5	8280.8664	0.002
25	-1	0	25.5	26	1	0	25.5	8281.2048	0.002
26	1	0	26.5	27	-1	0	26.5	8281.5542	0.002
27	-1	0	27.5	28	1	0	27.5	8281.9139	0.002
28	1	0	28.5	29	-1	0	28.5	8282.2845	0.002
30	1	0	30.5	31	-1	0	30.5	8283.0575	0.002
31	-1	0	31.5	32	1	0	31.5	8283.4597	0.002

References

[1] A. C. Vutha, W. C. Campell, Y. V. Gurevich, N. R. Hutzler, M. F. Parsons, D. Patterson, E. Pietrik, B. Spaun, J. M. Doyle, G. Gabrielse, and D. DeMille. Search for the electric dipole moment of the electron with thorium monoxide. *Journal of Physics B: Atomic, Molecular and Optical Physics*, 43(074007), 2010.

[2] J. Baron, W. C. Campell, D. DeMille, J. M. Doyle, G. Gabrielse, Y. V. Gurevich, P. W. Hess, N. R. Hutzler, E. Kirilov, I. Kozyryev, B. R. O'Leary, C. D. Panda, M. F. Parsons, E. S. Petrik, B. Spaun, A. C. Vutha, and A. D. West. Order of magnitude smaller limit on the electric dipole moment of the electron. *Science*, 343:269–272, 2014.

[3] Chad Orzel. Measuring (almost) zero. *Physics World*, pages 23–27, December 2009.

[4] B. L. Roberts. Historical introduction to electric and magnetic moments. In B. L. Roberts and W. J. Marciano, editors, *Lepton Dipole Moments*, volume 20 of *Advanced Series on Directions in High Energy Physics Series*, chapter 1, pages 1–9. World Scientific Publishing Co. Pte. Ltd., 2009.

[5] Alexander L. Baum. *High Resolution Rotational Spectroscopy Study of the Zeeman Effect in the* $^2\Pi_{1/2}$ *Molecule PbF.* B.A. Thesis for Pomona College, 2010.

[6] D. DeMille. Diatomic molecules, a window onto fundamental physics. *Physics Today*, 68(12), 2015.

[7] E. D. Commins and D. DeMille. The electric dipole moment of the electron. In B. L. Roberts and W. J. Marciano, editors, *Lepton Dipole Moments*, volume 20 of *Advanced Series on Directions in High Energy Physics Series*, chapter 14, pages 519–581. World Scientific Publishing Co. Pte. Ltd., 2009.

[8] Lukas D. Alphei, Jens-Uwe Grabow, A. N. Petrov, Richard Mawhorter, Benjamin Murphy, Alexander L. Baum, Trevor J. Sears, T. Zh. Yang, P. M. Rupasinghe, C. P. McRaven, and N. E. Shafer-Ray. Precision spectroscopy of the $^{207}Pb^{19}F$ molecule: Implications for measurement of P-odd and T-odd effects. *Physical Review A*, 83(040501), 2011.

[9] L. V. Skripnikov, A. D. Kudashov, A. N. Petrov, and A. V. Titov. Search for parity- and time-and-parity-violation effects in lead monofluoride (PbF): *Ab initio* molecular study. *Physical Review A*, 90(064501), 2014.

[10] M. G. Kozlov, V. I. Fomichev, Yu Yu Dmitriev, L. N. Labzovsky, and A. V. Titov. Calculation of the P- and T-odd spin-rotational Hamiltonian of the PbF molecule. *J. Phys. B: At. Mol. Phys*, 20:4939–4948, 1987.

[11] C. S. Wood, S. C. Bennett, D. Cho, B. P. Masterson, J. L. Roverts, C. E. Tanner, and C. E. Wieman. Measurement of parity nonconservation and an anapole moment in cesium. *Science*, 275:1759–1763, 1997.

[12] K. Balasubramanian. Relativistic configuration interaction calculations of low-lying states of PbF. *The Journal of Chemical Physics*, 83(2311), 1985.

[13] Richard J. Mawhorter, Benjamin S. Murphy, Alexander L. Baum, Trevor J. Sears, T. Zh. Yang, R. M. Rupasinghe, C. P. McRaven, N. E. Shafer-Ray, Lukas D. Alphei, and Jens-Uwe Grabow. Characterization of the ground X_1 state of $^{204}Pb^{19}F$, $^{206}Pb^{19}F$, $^{207}Pb^{19}F$, and $^{208}Pb^{19}F$. *Physical Review A*, 84(022508), 2011.

[14] K. Ziebarth, K. D. Setzer, O. Shestakov, and E. H. Fink. High-resolution study of the $X_2\ ^2\Pi_{3/2} \rightarrow X_1\ ^2\Pi_{1/2}$ fine structure transitions of PbF and PbCl. *Journal of Molecular Spectroscopy*, 191:108–116, 1998.

[15] P. Sivakumar, c. P. McRaven, P. M. Rupasinghe, T. Zh. Yang, N. E. Shafer-Ray, Trevor J. Sears, and Gregory E. Hall. Pseudo-continuous resonance enhanced multiphoton ionisation: Application to the determination of the hyperfine constants of $^{208}Pb^{19}F$. *Molecular Physics*, 108:927–935, 2010.

[16] C. P. McRaven, P. Sivakumar, and N. E. Shafer-Ray. Experimental determination of the hyperfine constants of the X_1 and A states of $^{207}Pb^{19}F$. *Physical Review A*, 78(054502), 2008.

[17] Lukas D. Alphei. *Elektronen- und Kern-Spinkopplungen im Rotationsspektrum des $^2\Pi_{1/2}$-Zustands von Bleifluorid*. Diplomarbeit Leibniz Universität Hannover, 2010.

[18] James K. G. Watson. The isotope dependence of the equilibrium rotational constants in $^1\Sigma$ states of diatomic molecules. *Journal of Molecular Spectroscopy*, 45:99–113, 1973.

[19] Robert J. Le Roy. Improved parameterization for combined isotopomer analysis of diatomic spectra and its application to HF and DF. *Journal of Molecular Spectroscopy*, 194:189–196, 1999.

[20] Brian J. Drouin, Harshal Gupta, Shanshan Yu, Charles E. Miller, and Holger S. P. Müller. High resolution spectral analysis of oxygen. II. Rotational spectra of $a^1\Delta_g$ O_2 isotopologues. *J Chem Phys*, 137(024305), July 2012.

[21] Zachary Glassman. *High Resolution Spectroscopy and Isotope Invariant Analysis of Diatomic Molecules*. B. A. Thesis for Pomona College, 2014.

[22] Zachary Glassman, Richard Mawhorter, Jens-Uwe Grabow, Anh Le, and Timothy C. Steimle. The hyperfine interaction in the odd isotope of ytterbium fluoride, ^{171}YbF. *Journal of Molecular Spectroscopy*, 300:7–11, 2014.

[23] David Griffiths. *Introduction to Elementary Particles*. WILEY-VCH Verlag GmbH & Co., Weinheim, second edition, 2011.

[24] Bradley Filippone. Searching for the neutron's electric dipole moment (EDM). Pomona College Physics Colloquium, Claremont, CA, Sept. 2015.

[25] David Griffiths. *Introduction to Electrodynamics*. Pearson Education, third edition, 2005.

[26] J. J. Hudson, D. M. Kara, I. J. Smallman, B. E. Sauer, M. R. Tarbutt, and E. A. Hinds. Improved measurement of the shape of the electron. *Nature*, 473:493–496, May 2011.

[27] Kevin C. Cossel, Daniel N. Gresh, Laura C. Sinclair, Tyler Coffey, Leonid V. Skripnikov, Alexander N. Petrov, Nikolai S. Mosyahin, Anatoly V. Titov, Rover W. Field, Edmund R. Meye, Eric A. Cornell, and Jun Ye. Broadband velocity modulation spectroscopy of HfF^+ : Towards a measurement of the electron electric dipole moment. *Chemical Physics Letters*, 546:1–11, 2012.

[28] J. J. Hudson, B. E. Sauer, M. R. Tarbutt, and E. A. Hinds. Measurement of the electron electric dipole moment using YbF molecules. *Physical Review Letters*, 89(2):023003, July 2002.

[29] H. Loh, K. C. Cossel, M. C. Grau, K.-K. Ni, E. R. Meyer, J. L. Bohn, J. Ye, and E. A. Cornell. Precision spectroscopy of polarized molecules in an ion trap. *Science*, 342(1220), 2013.

[30] L. V. Skripnikov and A. V. Titov. Theoretical study of ThF^+ in the search for T,P-violation effects: Effective state of a Th atom in ThF^+ and ThO compounds. *Physical Review A*, 91(042504), 2015.

[31] Takeshi Fukuyama. Searching for new physics beyond the standard model in electric dipole moment. *International Journal of Modern Physics A*, A27, 2012.

[32] M. Pospelov and A. Ritz. Probing CP violation with electric dipole moments. In B. L. Roberts and W. J. Marciano, editors, *Lepton Dipole Moments*, volume 20 of *Advanced*

Series on Directions in High Energy Physics Series, chapter 13, pages 439–518. World Scientific Publishing Co. Pte. Ltd., 2009.

[33] C. A. Baker, D. D. Doyle, P. Geltenbort, K. Green, M. G. D. van der Grinten, P. G. Harris, P. Iaydjiev, S. N. Ivanov, D. J. R. May, J. M. Pendlebury, J. D. Richardson, D. Shiers, and K. F. Smith. Improved experimental limit on the electric dipole moment of the neutron. *Physical Review Letters*, 97(13):131801, September 2006.

[34] S. K. Lamoreaux and R. Golub. The neutron electric dipole moment: Yesterday, today, and tomorrow. In B. L. Roberts and W. J. Marciano, editors, *Lepton Dipole Moments*, volume 20 of *Advanced Series on Directions in High Energy Physics Series*, chapter 15, pages 583–634. World Scientific Publishing Co. Pte. Ltd., 2009.

[35] V. V. Flambaum, D. DeMille, and M. G. Kozlov. Time-reversal symmetry violation in molecules induced by nuclear magnetic quadrupole moments. *Physical Review Letters*, 113(103003), 2014.

[36] L. V. Skripnikov, A. N. Petrov, N. S. Mosyagin, A. V. Titov, and V. V. Flambaum. TaN molecule as a candidate for the search for a T,P-violating nuclear magnetic quadrupole moment. *Physical Review A*, 92(012521), 2015.

[37] Timo Fleig, Malaya K. Nayak, and Mikhail G. Kozlov. TaN, a molecular system for probing P,T-violating hadron physics. *Physical Review A*, 93(012505), 2016.

[38] L. V. Skripnikov, A. N. Petrov, A. V. Titov, and V. V. Flambaum. CP-Violating effect of the Th nulcear magnetic quadrupole moment: Accurate many-body study of ThO. *Physical Review Letters*, 113(263006), December 2014.

[39] Jacob L. Bouchard, Timothy C. Steimle, Damian L. Kokkin, David J. Sharfi, and Richard J. Mawhorter. Branching ratios, radiative lifetimes, and transition dipole moments of tantalum nitride, TaN. *Physical Review A*, Submitted, 2016.

[40] John K. Bates and Dieter M. Gruen. The electronic and vibrational absorption spectrum of tantalum nitride (TaN) isolated in an argon matrix. *The Journal of Chemical Physics*, 70(4428), 1979.

[41] R. S. Ram, J. Liévin, and P. F. Bernath. Emission spectroscopy and *ab initio* calculations for TaN. *Journal of Molecular Spectroscopy*, 215:275–284, 2002.

[42] Walter Gordy and Robert L. Cook. *Microwave Molecular Spectra*. John Wiley & Sons, 1984.

[43] N. J. Stone. Table of nuclear magnetic dipole and electric quadrupole moments. *Atomic Data and Nuclear Data Tables*, 90:75–176, May 2005.

[44] Timothy C Steimle, Tongmei Ma, and Colan Linton. The hyperfine interaction in the $A^2\Pi_{1/2}$ and $X^2\Sigma^+$ states of ytterbium monofluoride. *J Chem Phys*, 127(234316), Dec 2007.

[45] L. F. Pašteka, R. J. Mawhorter, and P. Schwerdtfeger. Relativistic coupled-cluster calculations of the ^{173}Yb nuclear quadrupole coupling constant for the YbF molecule. *Molecular Physics*, 114(7-8), 2016.

[46] E. R. Cohen. *Quantities, Unites and Symbols in Physical Chemistry*. Royal Society of Chemistry (Great Britain), International Union of Pure, Applied, Physical, and Biophysical Chemistry Division, 2007.

[47] S.I. Sukhoruchkin and Z.N. Soroko. *Nuclei with Z = 55 - 100*, chapter Atomic Mass and Nuclear Binding Energy for Pb-205 (Lead), pages 6890–6892. Springer Berlin Heidelberg, Berlin, Heidelberg, 2009.

[48] A. N. Petrov, L. V. Skripnikov, A. V. Titov, and R. J. Mawhorter. Centrifugal correction to hyperfine structure constants in the ground state of lead monofluoride. *Physical Review A*, 88(010501), 2013.

[49] L. V. Skripnikov, A. N. Petrov, A. V. Titov, R. J. Mawhorter, A. L. Baum, T. J. Sears, and J.-U. Grabow. Further investigation of g factors for the lead monofluoride ground state. *Physical Review A*, 92(032508), 2015.

[50] Private Correspondence with N. E. Shafer-Ray.

[51] Shanshan Yu, Charles E. Miller, Brian J. Drouin, and Holger S. P. Müller. High resolution spectral analysis of oxygen. I. Isotopically invariant Dunham fit for the $X^3\Sigma_g^-, a^1\Delta_g, b^1\Sigma_g^+$ states. *The Journal of Chemical Physics*, 137:024304, 2012.

[52] Barbara M Giuliano, Luca Bizzocchi, Stephen Cooke, Deike Banser, Mareike Hess, Juliane Fritzsche, and Jens-Uwe Grabow. Pure rotational spectra of PbSe and PbTe: potential function, Born-Oppenheimer breakdown, field shift effect and magnetic shielding. *Phys Chem Chem Phys*, 10(15):2078–88, 2008.

[53] V. V. Flambaum, Y. V. Stadnik, M. G. Kozlov, and A. N. Petrov. Enhanced effects of temporal variation of the fundamental constants in $^2\pi_{1/2}$-term diatomic molecules: ^{207}Pb^{19}F. *Physical Review A*, 88(052124), 2013.

[54] Brian J. Drouin, Charles E. Miller, Holger S. P. Müller, and Edward A. Cohen. The rotational spectra, isotopically independent parameters, and interatomic potentials for the $X_1\ ^2\Pi_{3/2}$ and $X_2\ ^2\Pi_{1/2}$ states of BrO. *Journal of Molecular Spectroscopy*, 205:128–138, 2001.

[55] K. Ziebarth, R. Breidohr, O. Shestakov, and E. H. Fink. The $X_2\ ^2\Pi_{3/2} \rightarrow X_1\ ^2\Pi_{1/2}$ electronic band systems of lead monohalides in the near infrared. *Chemical Physics Letters*, 190:271–278, March 1992.

[56] Jens-Uwe Grabow, E. Samuel Palmer, Michael C. McCarthy, and Patrick Thaddeus. Supersonic-jet cryogenic-resonator coaxially oriented beam-resonator arrangement fourier transform microwave spectrometer. *Review of Scientific Instruments*, 76(9), 2005.

[57] Jens-Uwe Grabow, Wolfgang Stahl, and Helmut Dreizler. A multioctave coaxially oriented beam-resonator arrangement Fourier-transform microwave spectrometer. *Review of Scientific Instruments*, 67(12), 1996.

[58] Alberto Lesarri, R. D. Suenram, and Dale Brugh. Rotational spectrum of jet-cooled HfO_2 and HfO. *J Chem Phys*, 117(9651), 2002.

[59] Documentation for SPFIT and SPCAT. `https://www.astro.uni-koeln.de/site/vorhersagen/pickett/spinv.pdf`.

[60] Carson Witte. *Diatomic Molecular Spectroscopy of Potassium Iodide*. B. A. Thesis for Pomona College, 2016.

[61] Corey J Evans, Lisa-Maria E Needham, Nicholas R Walker, Hansjochen Köckert, Daniel P Zaleski, and Susanna L Stephens. The pure rotational spectra of the open-shell diatomic molecules PbI and SnI. *J Chem Phys*, 143(24), Dec 2015.

[62] Private Correspondence with Lukáš Pašteka and Peter Schwerdtfeger.

[63] Private Correspondence with E. H. Fink.